

- phase matching for third-harmonic generation," *Appl. Phys. Lett.*, vol. 27, pp. 390-392, Oct. 1, 1975.
- [246] A. H. Kung, J. F. Young, and S. E. Harris, "Generation of 1182 Å radiation in phase-matched mixtures of inert gases," *Appl. Phys. Lett.*, vol. 22, pp. 301-302, Mar. 15, 1973. See also errata, *Appl. Phys. Lett.*, vol. 28, p. 294, Mar. 1, 1976.
- [247] R. T. Hodgson, P. P. Sorokin, and J. J. Wynne, "Tunable coherent vacuum-ultraviolet generation in atomic vapors," *Phys. Rev. Lett.*, vol. 32, pp. 343-346, Feb. 1974.
- [248] J. A. Armstrong and J. J. Wynne, "Autoionizing states of Sr studied by the generation of tunable vacuum uv radiation," *Phys. Rev. Lett.*, vol. 33, pp. 1183-1185, Nov. 11, 1974.
- [249] S. E. Harris and D. M. Bloom, "Resonantly two-photon pumped frequency converter," *Appl. Phys. Lett.*, vol. 24, pp. 229-230, Mar. 1, 1974.
- [250] D. M. Bloom, J. T. Yardley, J. F. Young, and S. E. Harris, "Infrared up-conversion with resonantly two-photon pumped metal vapors," *Appl. Phys. Lett.*, vol. 24, pp. 427-428, May 1, 1974.
- [251] A. H. Kung, "Generation of tunable picosecond VUV radiation," *Appl. Phys. Lett.*, vol. 25, pp. 653-654, Dec. 1, 1974.
- [252] G. C. Bjorklund, "Effects of focusing on third-order nonlinear processes in isotropic media," *IEEE J. Quantum Electron.*, vol. QE-11, pp. 287-296, June 1975.
- [253] S. E. Harris, "Generation of vacuum-ultraviolet and soft-X-ray radiation using high-order nonlinear optical polarizabilities," *Phys. Rev. Lett.*, vol. 31, pp. 341-344, Aug. 6, 1973.
- [254] S. E. Harris, J. F. Young, A. H. Kung, D. M. Bloom, and G. C. Bjorklund, "Generation of ultraviolet and vacuum ultraviolet radiation," in *Laser Applications to Optics and Spectroscopy*, S. F. Jacobs, M. Sargent, III, J. F. Scott, and M. O. Scully, Eds. Reading, Mass.: Addison Wesley, 1975, vol. 2, pp. 181-197. See also E. A. Stappaerts, "Harmonic generation at high field strengths. Frequency shifts and saturation phenomena," *Phys. Rev. A*, vol. 11, pp. 1664-1667, May 1975.
- [255] P. Eisenberger and S. L. McCall, "X-ray parametric conversion," *Phys. Rev. Lett.*, vol. 26, pp. 684-688, Mar. 22, 1971.
- [256] P. M. Eisenberger and S. L. McCall, "Mixing of X-ray and optical photons," *Phys. Rev. A*, vol. 3, pp. 1145-1151, Mar. 1971.
- [257] S. E. Harris and D. B. Lidow, "Nonlinear optical processes by Van der Waals interaction during collision," *Phys. Rev. Lett.*, vol. 33, pp. 674-676, Sept. 16, 1974.
- [258] A. Ferguson, "How to make an X-ray laser," *New Scientist*, vol. 67, pp. 207-209, Oct. 23, 1975.
- [259] D. E. Eastman and M. I. Nathan, "Photoelectron spectroscopy," *Phys. Today*, vol. 28, pp. 44-51, Apr. 1975.
- [260] H. D. Jones, D. Eccleshall, and J. K. Temperley, "Propagation Characteristics of narrow X-ray pulses," U.S. Army Ballistic Research Lab., Rep. no. 1781, May 1975.
- [261] R. Hofstadter, "The Atomic Accelerator," Stanford Univ. High Energy Physics Lab., Stanford, CA, Rep. 560, Apr. 23, 1968.
- [262] P. V. Lenzo and E. G. Spencer, "High-speed low-power X-ray lithography," *Appl. Phys. Lett.*, vol. 24, pp. 289-291, Mar. 15, 1974.
- [263] T. Zehnpfennig, R. Giacconi, R. Haggerty, W. Reidy and G. Vaiana, "A laboratory program to develop improved grazing incidence X-ray optics," National Aeronautics and Space Administration, Rep. NASA-CR-717, Feb. 1967.
- [264] A. V. Baez, "Fresnel zone plate for optical image formation using extreme ultraviolet and soft X-radiation," *J. Opt. Soc. Amer.*, vol. 51, pp. 405-412, Apr. 1961.
- [265] C. D. Pfeifer, L. D. Ferris, and W. M. Yen, "Optical image formation with a Fresnel zone plate using vacuum-ultraviolet radiation," *J. Opt. Soc. Amer.*, vol. 63, pp. 91-95, Jan. 1973.
- [266] B. Niemann, D. Rudolph and G. Schmahl, "Soft X-ray imaging zone plates with large zone numbers for microscopic and spectroscopic applications," *Opt. Commun.*, vol. 12, pp. 160-163, Oct. 1974.
- [267] E. Spiller and A. Segmüller, "Propagation of X-rays in waveguides," *Appl. Phys. Lett.*, vol. 24, pp. 60-61, Jan. 15, 1974.
- [268] G. C. Bjorklund, S. E. Harris, and J. F. Young, "Vacuum ultraviolet holography," *Appl. Phys. Lett.*, vol. 25, pp. 451-452, Oct. 15, 1974.

An Introduction to Digital Matched Filters

GEORGE L. TURIN, FELLOW, IEEE

Abstract—In this introductory exposition, the class of noncoherent digital matched filters (DMF's) which are matched to AM signals is analyzed. Attention is focused on the special case of binary signals and one-bit digitization. Expressions are obtained relating output and input signal-to-noise ratios when the channel interference is additive and a) white Gaussian, b) incoherent and of constant amplitude, and c) coherent and of constant amplitude. These expressions are compared with expressions for the performance of the corresponding noncoherent analog matched filter under the same conditions. Improvements in DMF performance obtained by threshold biasing and by dithering are investigated; it is shown that DMF's can be made to outperform analog matched filters by proper use of the former technique. All theoretical results are corroborated by computer simulation.

Manuscript received October 24, 1975; revised February 23, 1976. This work was supported in part by the U.S. Army Electronics Command, through the Army Research Office, under Task Orders 72-734 and 74-379, and in part by the National Science Foundation under Grant ENG72-04128-A02.

The author is with the Department of Electrical Engineering and Computer Sciences and the Electronics Research Laboratory, University of California, Berkeley, CA 94720.

I. INTRODUCTION

ALTHOUGH THE CONCEPT of matched filters is now three decades old, their use has been confined largely to sophisticated and expensive systems. One problem has been that the very characteristic which makes matched filters valuable—a large time-bandwidth (TW) product—also has made them very difficult to fabricate in production quantities.

The advent of surface-acoustic-wave delay lines (SAWDL's) and large-scale integration (LSI) of digital circuits has completely changed the picture. On the one hand, it is now commonplace to fabricate, with high replicability, SAWDL matched filters with TW products of several hundred [1]. On the other hand, digital versions of matched filters with TW products of several hundred can be achieved on one or a few LSI chips.

The communication system designer can therefore begin to think of matched filters of considerable complexity as "off-

the-shelf" items. Whether he uses an analog device, such as a SAWDL, or a digital device will depend on the particular application. For example, when the only interference encountered in the communication (or radar) system is Gaussian noise, an analog realization will be the more desirable. However, as we shall see, when malevolent jamming and/or real-time signal programmability are at issue, it may be preferable to utilize a digital matched filter (DMF).

From an analytical viewpoint, analog matched filters are thoroughly understood [2], [3]. Digital matched filters are not as well understood, even though the literature on them and on related digital correlators is substantial (e.g., [4]-[6]). The purpose of the present paper is to clarify, unify, and extend the analysis of a common class of DMF's, those matched to AM signals. Although some of the results presented here have previously been reported, it is believed that many of our results, our approach, our concentration on the *noncoherent* DMF, and our analysis of certain biased and adaptive threshold techniques are novel.

Only the case of binary signals, additive interference, and binary digitization is scrutinized in this paper. An extension of the results to multilevel digitization will be given in a later paper. Still other work is proceeding on the performance of DMF's matched to more general signals, faced with nonadditive interference, having adaptive capabilities, etc.

In the present paper, we review certain fundamental properties of coherent and noncoherent analog matched filters in Section II; this material forms the background for a discussion of DMF's. The operation of a class of noncoherent DMF's is described in Section III. The signal-to-noise ratio (SNR) performance of such DMF's is derived in Section IV for the case of binary signalling and one-bit zero-threshold digitization, when the interference in the channel is white Gaussian noise or is constant-amplitude jamming. The effects of threshold bias are determined in Section V, where optimal, suboptimal, and adaptive thresholds are considered. Dithering is discussed in Section VI. Finally, all the analytical results of the paper are brought together in graphical form in Section VII, where the results of corroborating simulation runs are also presented.

II. REVIEW OF MATCHED FILTER THEORY

In this section, we review certain of the principal aspects of analog matched-filter theory [2] as a basis for our analysis of DMF's.

A. The Coherent Channel

Let $s(t)$, $0 \leq t \leq T$, be a signal to which a filter is to be matched. The impulse response of the matched filter is defined to be [2]

$$h(\tau) \triangleq \begin{cases} ks(T - \tau), & 0 \leq \tau \leq T \\ 0, & \text{elsewhere} \end{cases} \quad (1)$$

where the gain factor k is arbitrary and is henceforth taken as unity. If $s(\cdot)$, together with the additive interference $n(\cdot)$, is passed into the matched filter of (1), the filter's output is given by

$$y(t) = \int_0^T s(T - \tau) s(t - \tau) d\tau + \int_0^T s(T - \tau) n(t - \tau) d\tau. \quad (2)$$

The signal component of $y(\cdot)$, i.e., the first term of (2), reaches its maximum at $t = T$. A measure of how much this signal peak of $y(\cdot)$ protrudes above the noise in $y(\cdot)$ is the

output SNR

$$\text{SNR}_o \triangleq \frac{\{E_S[y(T)] - E_{NS}[y(T)]\}^2}{\text{var}_S[y(T)]}. \quad (3)$$

In (3), $E[\cdot]$ stands for mean value and $\text{var}[\cdot]$ for variance; the subscripts S and NS condition these averages on "signal present" and "signal absent," respectively, i.e., whether the first term in (2) is present or absent. SNR_o is a key parameter of matched-filter performance.

When the interference $n(\cdot)$ is stationary with spectral density $\hat{N}(f)$, $-\infty < f < \infty$, SNR_o is easily shown to be [3]

$$\text{SNR}_o = \frac{\mathcal{E}^2}{\int_{-\infty}^{\infty} \hat{N}(f) |\hat{S}(f)|^2 df} \quad (4)$$

where

$$\mathcal{E} \triangleq \int_0^T s^2(t) dt \quad (5)$$

is the signal's energy and $\hat{S}(\cdot)$ is the Fourier transform of $s(\cdot)$. Appendix A gives values of SNR_o for several combinations of interference and signal spectra. In particular, when the interference is white, i.e., $\hat{N}(f) \equiv N_o/2$, the familiar formula

$$\text{SNR}_o = \frac{2\mathcal{E}}{N_o} = 2\text{TW}(\text{SNR}_i) \quad (6)$$

results, independently of the shape of the signal spectrum. In (6), W is the noise bandwidth [7, p. 201] (see Appendix B) of the matched filter. $\text{SNR}_i \triangleq P_i/N_i$ is the effective input SNR, where

$$P_i \triangleq \mathcal{E}/T \quad (7)$$

is the signal power over $0 \leq t \leq T$ and

$$N_i \triangleq N_o \text{W} \quad (8)$$

is the input noise power contained in a W Hz bandwidth.

The second equality of (6), which shows an input-to-output SNR gain of 2TW , has been largely responsible for 30 years of effort to achieve ever-larger TW products. This is ironical, since the first equality of (6) clearly shows that all signals with a given energy perform equally well, irrespective of their TW products. In fact, the desirability of large values of TW is real but stems from other considerations, e.g.:

- 1) requirements for small peak and/or average signal power, which lead to spreading the energy \mathcal{E} over a large interval T ;
- 2) requirements for high time/velocity resolution in radar and synchronizing systems [2];
- 3) the need for high path resolvability in antilmultipath systems [8];
- 4) the desire in security systems to avoid detection or interception of one's signal, which leads to time- and frequency-spreading techniques;
- 5) strategies to force spectral dispersion of a jammer's power¹ [3].

¹ Note the difference between natural white noise and white jamming. The former has virtually unlimited power and bandwidth, so spectrum spreading of the signal merely increases W and therefore N_i of (8) without changing SNR_o . The latter has finite power, so increasing W forces a decrease of N_o in (8), hence an increase in SNR_o of (6).

Thus the effort to achieve a large TW is not misdirected, and SAWDL and digital LSI techniques for accomplishing this end are truly a boon.

B. The Noncoherent Channel

In most radio-frequency applications, the signal is subjected to an additional perturbation—randomization of its carrier phase. Although restoration of phase coherence is feasible, the more customary procedure, fully justified by theory (see, e.g., [9, pp. 49 *et seq.*]), is to follow the matched filter with an envelope detector.

The performance of the matched filter-envelope detector combination can be analyzed by first writing $s(\cdot)$ and $n(\cdot)$ in familiar bandpass form:

$$s(t) = S(t) \cos(\omega_0 t + \theta(t)) \quad (9)$$

$$n(t) = N(t) \cos(\omega_0 t + \phi(t)). \quad (10)$$

Here, ω_0 is an appropriately chosen “center” frequency (usually the carrier frequency) and $S(\cdot)$, $N(\cdot)$, $\theta(\cdot)$, and $\phi(\cdot)$ are low-pass waveforms representing amplitude and phase fluctuations; $\theta(\cdot)$ also includes any phase shift imparted to $s(\cdot)$ by the channel. If (9) and (10) are used in (2), trigonometric identities applied, and integrals involving double-frequency terms ignored in the usual manner, equation (2) becomes

$$\begin{aligned} y(t) = & \frac{1}{2} \left\{ \int_0^T S(\tau)S(\tau - \alpha) \cos[\theta(\tau) - \theta(\tau - \alpha)] d\tau \right. \\ & + \left. \int_0^T S(\tau)N(\tau - \alpha) \cos[\theta(\tau) - \phi(\tau - \alpha)] d\tau \right\} \cos \omega_0 \alpha \\ & - \frac{1}{2} \left\{ \int_0^T S(\tau)S(\tau - \alpha) \sin[\theta(\tau) - \theta(\tau - \alpha)] d\tau \right. \\ & + \left. \left. \int_0^T S(\tau)N(\tau - \alpha) \sin[\theta(\tau) - \phi(\tau - \alpha)] d\tau \right\} \sin \omega_0 \alpha \right\} \quad (11) \end{aligned}$$

where $\alpha \triangleq T - t$. Denoting the four integrals in (11) by I_1 , I_2 , I_3 , and I_4 , respectively, we can define the envelope of $y(t)$ as

$$y_e(t) \triangleq \frac{1}{2} \sqrt{[I_1(\alpha) + I_2(\alpha)]^2 + [I_3(\alpha) + I_4(\alpha)]^2}. \quad (12a)$$

At $t = T$ ($\alpha = 0$), this becomes

$$y_e(T) = \frac{1}{2} \sqrt{[I_1(0) + I_2(0)]^2 + I_4^2(0)} \quad (12b)$$

since $I_3(0) = 0$. If SNR_o is large ($\text{SNR}_o \gg 1$), $I_2(0)$ and $I_4(0)$ are clearly small compared to $I_1(0)$, so

$$y_e(T) \cong \frac{1}{2} |I_1(0) + I_2(0)| \cong y(T) \quad (13)$$

where the second approximation recognizes that, for $\text{SNR}_o \gg 1$, $I_1(0) + I_2(0)$ is positive with high probability. The near identity of $y_e(T)$ and $y(T)$ for a large SNR_o implies that the large- SNR_o performance of the matched filter-envelope detector combination is little changed from that of the matched filter alone. In particular, when the noise is white and $\text{SNR}_o \gg 1$, equation (6) still holds very closely for the non-coherent arrangement.

It is often convenient to work with $z \triangleq y_e^2$ rather than y_e , i.e., to use a square-law envelope detector. Since z and y_e are related in a one-to-one manner, no information is lost by this transformation, and one should expect no degradation of performance, as measured by, say, the probability of error in making a hard decision based on z . This expectation is substantiated by analysis [9]. However, since the statistics of z are different from those of y_e , the SNR obtained by applying (3) to z rather than to y_e will of course change. In fact, as is shown in Appendix C, when $\text{SNR}_o \gg 1$,

$$\text{SNR}_o(z) \cong \frac{1}{4} \text{SNR}_o(y_e) \quad (14)$$

which reduces for white noise to (see (6))

$$\text{SNR}_o(z) \cong \frac{\frac{1}{2}}{2N_0} = \frac{\text{TW}}{2} (\text{SNR}_t). \quad (15)$$

Thus two systems, using y_e and the other z as output decision variables, while exhibiting identical performance in terms of probability of error, will show a factor-of-four (or 6 dB) difference in output SNR. This shows the danger in uncritical use of SNR_o as a performance measure, especially in the comparison of unlike systems.

Nonetheless, we shall use SNR_o as a performance measure for DMF's because of the ease of its evaluation. The danger is ameliorated by always analyzing a noncoherent square-law DMF and using $\text{SNR}_o(z)$, not $\text{SNR}_o(y_e)$, as a baseline of comparison. Even with such precautions, it must always be borne in mind that SNR_o is not a definitive measure and may be misleading in some cases.

C. Low-Pass Realization for AM Signals

A common realization of a noncoherent matched filter involves the low-pass “quadratures” technique. Although this technique can be used for arbitrary signals, we limit the discussion here to amplitude-modulated signals, since it is DMF's for such signals that we will analyze in this paper.

The quadratures technique is shown in block diagram form in Fig. 1. The input signal $s(\cdot) + n(\cdot)$ is first heterodyned down to low pass by the use of two sinusoids, at carrier frequency, which are in phase quadrature.² The low-pass waveforms are both then passed into filters which are matched to the signal amplitude $S(\cdot)$. The filter outputs are squared and added to form the waveform $\hat{y}_e^2(\cdot)$. It is shown in Appendix D that $\hat{y}_e(t) \equiv y_e(t)$, i.e., the device of Fig. 1 is equivalent to the corresponding bandpass matched filter-envelope detector combination discussed above. The output SNR for the device, at time $t = T$, is therefore given by (15).

The value of the low-pass quadratures technique of matched filtering is largely historical, since it has previously been easier to realize the two low-pass matched filters of Fig. 1 than the one corresponding bandpass matched filter. The advent of SAWDL's has completely reversed the situation, making Fig. 1 an obsolete technique in the analog-filtering case.

² The sinusoids frequency can in fact differ from the carrier frequency by some small fraction of $1/T$ without substantial modification of the behavior of the system. Note also that by setting $\theta(t) \equiv 0$, we have specified the received signal phase—which includes any channel phase shift—as the phase origin. Then η in Fig. 1 is the difference between the received signal phase and the receiver's phase; for the noncoherent system considered, η is a random variable which is uniformly distributed between 0 and 2π .

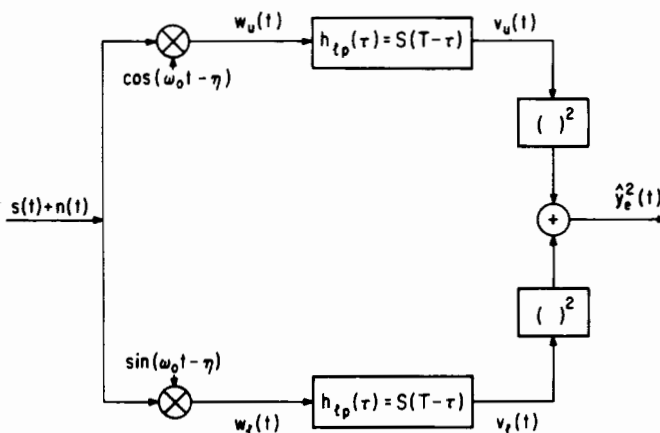


Fig. 1. Low-pass realization of analog matched filter for AM signal.

However, digital matched filters are still best realized at low pass, largely because of sampling-rate considerations. Therefore, Fig. 1 is the point from which we start our discussion of noncoherent DMF's. In all that follows, we assume that $s(\cdot)$ is purely amplitude modulated, which is the case to which Fig. 1 applies.

III. OPERATION OF DMF'S

As we shall see in later sections, it is not necessary to consider a DMF to be merely an approximation to an analog matched filter. Rather, it is more desirable to consider it in its own right, to be optimized as a nonlinear device. In this section, however, we approach the DMF from the former viewpoint.

From that viewpoint, the digital realization of Fig. 1 is most easily described by writing a succession of approximations to the convolution integrals characterizing the matched filters in the figure. Taking the upper filter, for example, we have

$$v_u(t) = \int_0^T S(T - \tau) w_u(t - \tau) d\tau. \quad (16)$$

The first approximation involves writing a sampled-data form of (16):

$$v_{uk} \cong \delta \sum_{i=0}^{L-1} S_{L-i} w_{u,k-i} \quad (17)$$

where $v_{uj} \triangleq v_u(j\delta)$, $w_{uj} \triangleq w_u(j\delta)$, and $S_j \triangleq S(j\delta)$ are samples of $v_u(\cdot)$, $w_u(\cdot)$, and $S(\cdot)$ taken every δ s, and $L\delta = T$. The sampling rate $1/\delta$ is a parameter of the system; it should be at least the Nyquist rate determined by the bandwidth of the low-pass components of the multiplier output waveforms of Fig. 1³ and perhaps greater if a finer time resolution is needed at the DMF output for ranging or synchronization.

The next approximation starts with writing binary expansions of the samples w_{uj} and S_j :

$$w_{uj} = \sum_{m=0}^{\infty} w_{uj}^m 2^{-m} \quad (18)$$

³The multiplier output waveforms also contain double-frequency terms at $2\omega_0$. As indicated by (11), these terms are suppressed by the low-pass analog filters themselves in Fig. 1. In the corresponding DMF, double-frequency suppression is accomplished by low-pass zonal filters after the multipliers, as shown in Fig. 3. We henceforth assume that $w_u(\cdot)$ and $w_l(\cdot)$ refer only to the low-pass components of the multiplier outputs.

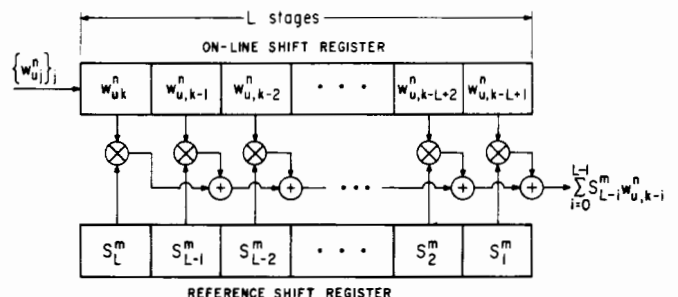


Fig. 2. A digital correlator.

and

$$S_j = \sum_{m=0}^{\infty} S_j^m 2^{-m} \quad (19)$$

In these expressions, w_{uj}^m and S_j^m , which take on the values ± 1 , are the m th digits of bipolar binary representations of the respective analog values. We have implicitly assumed that w_{uj} and S_j have been scaled so as to lie almost always in the -2 to $+2$ amplitude range;⁴ we adopt the convention that if an analog value is greater than $+2$ (less than -2) its binary representation consists of all $+1$'s (-1 's).

We now approximate the sums in (18) and (19) by truncating w_{uj} to M digits and S_j to N digits. Placing the truncated binary expansions in (17) and interchanging the order of the sums, we obtain

$$v_{uk} \cong \delta \sum_{m=0}^{M-1} \sum_{n=0}^{N-1} 2^{-(m+n)} \sum_{i=0}^{L-1} S_{L-i}^m w_{u,k-i}^n. \quad (20)$$

This expression describes a digital realization of the upper branch of Fig. 1. A similar expression holds for the lower branch and is obtained by replacing the subscripts u with l in (20).

In order to obtain an approximation to the sequence of samples of $v_u(\cdot)$ of (16), we therefore proceed as follows:

- 1) scale $w_u(\cdot)$ and $S(\cdot)$ to the range -2 to $+2$;
- 2) sample $w_u(\cdot)$ and $S(\cdot)$ every δ s;
- 3) digitize the samples into truncated binary forms;
- 4) correlate the m th digits of the binary expansions for the samples of $S(\cdot)$ against the n th digits of the binary expansions for $w_u(\cdot)$, thus performing MN correlations;
- 5) combine the correlations according to (20), using weights $2^{-(m+n)}\delta$.

If desired, the sequence of samples of $v_u(\cdot)$ thus obtained can be interpolated to form a continuous-time approximation to $v_u(\cdot)$ itself.

The scaling, sampling, and digitizing of $S(\cdot)$ is of course done once and for all, and the resultant digital values are stored in the receiver. The corresponding operations on $w_u(\cdot)$ are performed, respectively, by an automatic gain control, a sampler, and an N bit A/D converter. The correlation of step 4 is achieved by a shift-register device, as described below. Step 5 is achieved by a D/A converter with appropriate weights.

The shift-register device for performing digital correlations is shown in Fig. 2. The sequence of the n th digits of the expan-

⁴This can be asserted to be true only with high probability in the case of w_{uj} . It also implies the use of an automatic gain control in the system.

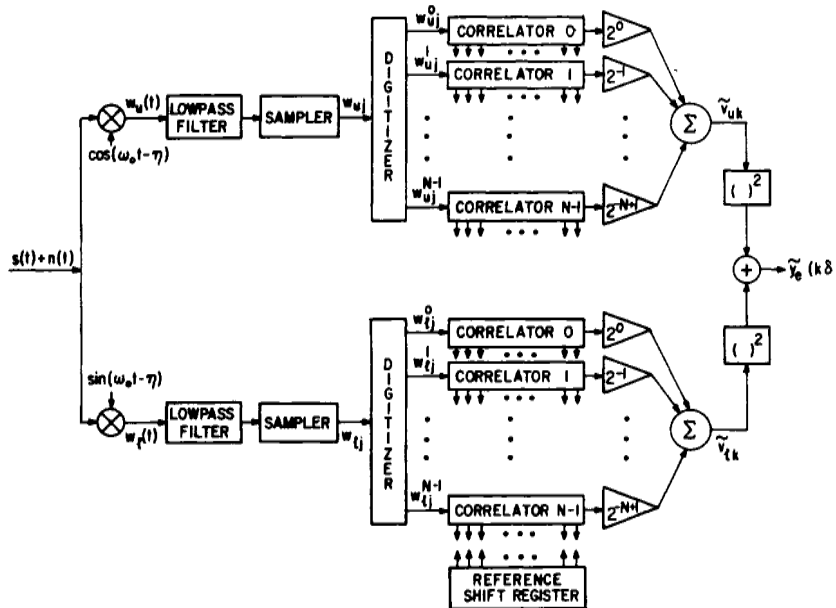


Fig. 3. Digital matched filter for binary signal.

sions of the w_{uj} samples is inserted into the upper shift register from the left. At each sample-clock pulse, the most-recent sample's n th digit enters the leftmost stage, all previous contents move one stage to the right, and the rightmost stage's previous content is discarded. The m th digits of the samples S_j are permanently stored in the stages of the lower, or reference, shift register.⁵ At each clock pulse, the contents of the two shift registers are multiplied in pairs and the products added.

A complete digital realization of the noncoherent matched filter of Fig. 1 thus involves $2N$ "on-line" shift registers (N for each branch in Fig. 1), M reference shift registers (which serve both branches), $2MN$ multipliers, and $2MN(L-1)$ adders, in addition to the heterodyning mixers, low-pass filters, samplers, A/D converters, D/A converters, squarers, and output adders. Until recently, such a mass of components was not practical even for small values of M , N , and L , except for the most sophisticated systems. LSI technology, however, now allows realization of entire DMF's on a few LSI chips for moderate values of M , N and L .

A block diagram of a DMF for arbitrary M and N would be difficult to draw, because of the $2MN$ sets of interconnections between the $2N$ on-line shift registers and the M reference shift registers. Fig. 3 shows a special case, where $M = 1$. In this figure, the correlators contain the on-line register and all of the multipliers and adders of Fig. 2 but not the reference register; the latter is shown separately and supplies the reference digits $\{S_j^0\}$ to all the correlators. In drawing Fig. 3, it is assumed that any automatic gain control precedes the DMF input. Further, for convenience, the gain factor δ called for in (20) has been left out of the weights $2^{-(m+n)}$, so \tilde{v}_{uk} , \tilde{v}_{ik} , and $\tilde{y}_e^2(k\delta)$ denote the DMF's approximations to v_{uk}/δ , v_{ik}/δ , and $y_e^2(k\delta)/\delta^2$, respectively.

The low-pass zonal filters mentioned in footnote 3 and shown in Fig. 3 are assumed to have flat gains over their low-

pass bands. While these filters can be optimized to improve the DMF's performance, such prefiltering has its disadvantages. First, the optimum prefilter depends on the character of the channel interference and should ideally be adaptive. (As a compromise, it is often matched to the elementary "chip" waveform, as discussed later.) Second, prefiltering distorts the waveform of the signal component of $w_{uj}(\cdot)$ (or $w_{ij}(\cdot)$), thus leading to the need for accurate timing of the samplers so as to obtain maximum predigitizer SNR. As indicated below, we have avoided both of these complications by using the zonal-filter approach; we will however, comment on prefiltering techniques in what follows.

The special case of Fig. 3 suffices for the present paper, since we consider here only binary signalling. For binary signalling, $S_j = \pm A$ (implying phase-shift keying), which on normalization can be scaled to ± 1 . Then (19) can be truncated to one term, i.e., $M = 1$.

A further specialization is applied in the present paper: the digitizers are truncated to $N = 1$, so Fig. 3 contains only two correlators. Effectively, only the polarities of w_{uj} and w_{ij} are retained, so the need for an automatic gain control for amplitude normalization of these quantities is eliminated.

The remainder of the paper is concerned only with this special case, $M = N = 1$. Subsequent papers will examine larger values of M and N .

IV. PERFORMANCE ANALYSIS

We now derive the output SNR for the noncoherent DMF of Section III, assuming one-bit digitization and binary signals, i.e., $M = N = 1$ in Fig. 3. Just as SNR_o of (15), for a noncoherent analog matched filter, was calculated at $t = T$, we shall compute SNR_o for the DMF at $k = L$, i.e., for the output sample

$$\begin{aligned} \tilde{z} &\triangleq \tilde{y}_e^2(L\delta) = \tilde{v}_{uL}^2 + \tilde{v}_{iL}^2 \\ &= \left[\left(\sum_{i=0}^{L-1} S_{L-i}^0 w_{u,L-i}^0 \right)^2 + \left(\sum_{i=0}^{L-1} S_{L-i}^0 w_{i,L-i}^0 \right)^2 \right]. \end{aligned} \quad (21)$$

⁵ Of course, the permanence of storage is flexible. A major advantage of the DMF is the ease of reprogramming; a change of the signal to which it is matched is accomplished by a simple reloading of the reference shift register(s) with the coefficients of the new signal.

In particular, we shall calculate SNR_o for three types of additive interference—Gaussian noise, incoherent constant-amplitude interference, and coherent constant-amplitude interference—and compare these SNR 's to the corresponding results for the analog filter, given in Appendix A.

We have specialized to phase-shift keying, $S(t) = \pm A$ ($A > 0$) for all t , and now assume that a new value of $S(\cdot)$ is transmitted once every δ s. Then $S(\cdot)$ is specified by L δ -s “chips,” each having a value of $+A$ or $-A$. Since the DMF's sampling rate is $1/\delta$, we see that the DMF's samplers take exactly one sample per chip. Because the low-pass zonal filters of Fig. 3 are assumed not to distort the rectangular chip waveshapes, the timing of the sampling is not critical, i.e., chip synchronization of the samplers is not required.

Starting with $s(\cdot)$ and $n(\cdot)$ of (9) and (10) as inputs to Fig. 3 and tracing through to the output of the sampler, it is easily shown that the samples during the j th chip are

$$w_{uj} = \frac{S_j}{2} \cos \eta + n_{uj} \quad (22)$$

$$w_{lj} = -\frac{S_j}{2} \sin \eta + n_{lj} \quad (23)$$

where $S_j = \pm A$ and

$$n_{uj} \triangleq \frac{N(j\delta)}{2} \cos [\phi(j\delta) + \eta] \quad (24)$$

$$n_{lj} \triangleq -\frac{N(j\delta)}{2} \sin [\phi(j\delta) + \eta]. \quad (25)$$

Since an unbiased one-bit digitizer⁶ is characterized by $y = \text{sgn } x$, where x is the digitizer input, y is its output, and

$$\text{sgn } x = \begin{cases} +1, & x > 0 \\ -1, & x < 0 \end{cases} \quad (26)$$

we can write \tilde{v}_{uL} and \tilde{v}_{lL} of (21) as

$$\tilde{v}_{uL} = \sum_{j=1}^L S_j^0 \text{sgn} \left[\frac{S_j}{2} \cos \eta + n_{uj} \right] \quad (27)$$

$$\tilde{v}_{lL} = \sum_{j=1}^L S_j^0 \text{sgn} \left[-\frac{S_j}{2} \sin \eta + n_{lj} \right] \quad (28)$$

where we have reordered the index of summation.

We now consider two cases of interest. In the first, the interference samples $n_{u1}, \dots, n_{uL}, n_{l1}, \dots, n_{lL}$ are symmetric, independent, and identically distributed (SIID). In the second case, the samples are still random variables, but stay constant from chip to chip: $n_{u1} = n_{u2} = \dots = n_{uL}; n_{l1} = n_{l2} = \dots = n_{lL}$.

A. SIID Interference Samples

Consider the summand of (27) and suppose that $S_j = +A$ so $S_j^0 = +1$. In order to have $\text{sgn}[A/2 \cos \eta + n_{uj}] = -1$, i.e., a disagreement between the digitized transmitted and received samples S_j^0 and w_{uj}^0 , we must have

$$n_{uj} < -\frac{A}{2} \cos \eta. \quad (29)$$

Similarly, if $S_j = -A$, disagreement occurs if

$$n_{uj} > \frac{A}{2} \cos \eta. \quad (30)$$

Let n_{uj} be a symmetric random variable so that the probabilities of events (29) and (30) are equal, and call this probability $p_u(\eta)$:

$$p_u(\eta) \triangleq \Pr \left[n_{uj} < -\frac{A}{2} \cos \eta \right]. \quad (31)$$

p_u is therefore the probability that a term in (27) equals -1 and $1 - p_u$ is the probability that it equals $+1$. If the n_{uj} 's are independent and identically distributed (IID), the terms in (27) are also IID, taking on the values ± 1 , and \tilde{v}_{uL} is binomially distributed.

The moment-generating function of \tilde{v}_{uL} is therefore [10, p. 219]

$$m(t) = [(1 - p_u)e^t + p_u e^{-t}]^L \quad (32)$$

and the moments of \tilde{v}_{uL} are

$$E[\tilde{v}_{uL}^k] = \frac{d^k m}{dt^k} \Big|_{t=0} \quad (33)$$

from which we have, after some manipulation,

$$E[\tilde{v}_{uL}^2] = L[(L-1)(1-2p_u)^2 + 1] \quad (34)$$

$$E[\tilde{v}_{uL}^4] = L[(L-1)(L-2)(L-3)(1-2p_u)^4 + 2(3L-4)(L-1)(1-2p_u)^2 + (3L-2)]. \quad (35)$$

Then

$$\text{var}(\tilde{v}_{uL}) = 2L(L-1)[(3-2L)(1-2p_u)^4 + 2(L-2)(1-2p_u)^2 + 1]. \quad (36)$$

Similar expressions are obtained for moments of \tilde{v}_{lL} by replacing p_u by

$$p_l(\eta) \triangleq \Pr[n_{lj} < \frac{A}{2} \sin \eta]. \quad (37)$$

Making use of the fact that the set of n_{uj} 's and the set of n_{lj} 's are independent, we thus find the mean and variance of \tilde{z} of (21) to be

$$E[\tilde{z}|\eta] = L\{(L-1)[(1-2p_u)^2 + (1-2p_l)^2] + 2\} \quad (38)$$

$$\text{var}(\tilde{z}|\eta) = 2L(L-1)\{(3-2L)[(1-2p_u)^4 + (1-2p_l)^4] + 2(L-2)[(1-2p_u)^2 + (1-2p_l)^2] + 2\} \quad (39)$$

where the condition on η recognizes the dependence of p_u and p_l on η . Since noncoherence implies that η is a random variable which is uniformly distributed on $(0, 2\pi]$ (see footnote 2) we have

$$E[\tilde{z}] = \frac{1}{2\pi} \int_0^{2\pi} E[\tilde{z}|\eta] d\eta \quad (40)$$

$$\begin{aligned} \text{var}[\tilde{z}] &= \frac{1}{2\pi} \int_0^{2\pi} \text{var}(\tilde{z}|\eta) d\eta \\ &\quad + \frac{1}{2\pi} \int_0^{2\pi} \{E[\tilde{z}|\eta] - E[\tilde{z}]\}^2 d\eta. \end{aligned} \quad (41)$$

⁶See Section V for the case of biased digitizers.

SNR_o can then be written, using (40) and (41), as

$$\text{SNR}_o = \frac{\{E_S[\tilde{z}] - E_{NS}[\tilde{z}]\}^2}{\text{var}_{S^2}(\tilde{z})}. \quad (42)$$

Gaussian Noise: As a first application of these results, we assume that the channel interference is white and Gaussian, with double-sided spectral density $N_o/2$. It is shown in Appendix E that $n_{u1}, \dots, n_{uL}, n_{l1}, \dots, n_{lL}$ of (24) and (25) are zero-mean Gaussian random variables (thus symmetric), approximately independent, with variance $\sigma^2 = N_o W/4$. (W here is the noise bandwidth of the DMF receiver's front end, which is assumed to be equal to the noise bandwidth of $s(\cdot)$, and hence of the associated analog matched filter; see Appendix B.) Then, from (31) and (37), we have

$$p_u(\eta) = \frac{1}{2} - \frac{1}{\sqrt{2\pi}\sigma} \int_0^{(A/2)\cos\eta} \exp\left(-\frac{x^2}{2\sigma^2}\right) dx \quad (43)$$

$$p_l(\eta) = \frac{1}{2} + \frac{1}{\sqrt{2\pi}\sigma} \int_0^{(A/2)\sin\eta} \exp\left(-\frac{x^2}{2\sigma^2}\right) dx. \quad (44)$$

The case of most interest is when SNR_i is small but SNR_o is large, for this is the case in which the matched filter has most value. Recall that $\text{SNR}_i \triangleq P_i/N_i$, where, from (5), (7), and (9)

$$P_i \cong \frac{1}{2T} \int_0^T S^2(t) dt = \frac{A^2}{2}. \quad (45)$$

Since W is now the receiver's front-end noise bandwidth, equation (8) still holds for N_i ; so

$$\text{SNR}_i \cong \frac{A^2}{2WN_o} = \frac{A^2}{8\sigma^2}. \quad (46)$$

If we assume that $\text{SNR}_i \ll 1$, then the integrands of (43) and (44) are approximately constant and equal to unity over the intervals of integration, and

$$1 - 2p_u(\eta) \cong \frac{A \cos \eta}{\sqrt{2\pi}\sigma} \quad (47)$$

$$1 - 2p_l(\eta) \cong -\frac{A \sin \eta}{\sqrt{2\pi}\sigma}. \quad (48)$$

Substituting these values in (38) and (39), applying (40) and (41), and using (42), we obtain

$$\text{SNR}_o = \frac{L(L-1)(A^2/2\sigma^2)^2}{2[(3-2L)(3A^4/32\pi^2\sigma^4) + 2(L-2)(A^2/2\sigma^2)^2 + 2]}. \quad (49)$$

In the region where $\text{SNR}_i = A^2/8\sigma^2 \ll 1$ but $\text{SNR}_o \gg 1$, equation (49) implies that $L \gg 1$ and reduces to

$$\text{SNR}_o \cong \frac{L}{2} \frac{A^2}{4\sigma^2} = \frac{2}{\pi} \left(\frac{TW}{2} \right) \text{SNR}_i \quad (50)$$

where we have used the fact that the noise bandwidth of a phase-shift-keyed signal is the reciprocal of the chip rate, i.e., $W = 1/\delta = L/T$. (See Appendix B.)

The result in (50) is well known [4]. It shows, on comparison with (15), that when $\text{SNR}_i \ll 1$, $\text{SNR}_o \gg 1$, and

the channel interference is white and Gaussian, a one-bit DMF suffers only about $10 \log_{10} \pi/2 \cong 2$ dB of degradation compared with the associated analog matched filter. Graphs of (49) and (50), and of other results below, are reserved for the final section.

Coherent Constant-Amplitude Interference: As a second application of the results of (38)–(42), we assume that the channel interference has constant amplitude, but that its phase is completely incoherent; more precisely, in (10) we set $N(t) \equiv J = \text{constant} \geq 0$ and assume that $\phi_j \triangleq \phi(j\delta)$ are independent random variables which are uniformly distributed over $(0, 2\pi]$. This type of interference can originate, e.g., from a sine-wave jammer at the carrier frequency ω_0 , whose phase is extremely unstable with respect to the receiver's phase η , or from a sine-wave jammer within the signal band but far enough removed from ω_0 so that its effective phase with respect to η changes substantially from chip to chip, or from a chirp jammer, etc. Amplitude keying ($N(t) = \pm J$) can additionally be overlaid upon any of these interference waveforms since this corresponds to additional $\pm\pi$ phase shifts.

From (24) and (25),

$$n_{uj} = \frac{J}{2} \cos [\phi(j\delta) + \eta] \quad (51)$$

$$n_{lj} = -\frac{J}{2} \sin [\phi(j\delta) + \eta]. \quad (52)$$

As required by (38)–(42), n_{u1}, \dots, n_{uL} are SIID, as are n_{l1}, \dots, n_{lL} . However, n_{uj} —although independent of n_{lk} , $k \neq j$ —is dependent on n_{lj} although uncorrelated from it. (See Appendix E.) \tilde{n}_{uL} and \tilde{n}_{lL} of (27) and (28) are therefore not completely independent, although one would expect the dependence to be slight for large L . The use of (38) and (39), which require complete independence, is still a good approximation.

There is no difficulty in showing from (31) and (37) that

$$p_u(\eta) = \begin{cases} 0, & \frac{A}{J} \cos \eta > 1 \\ \frac{1}{\pi} \cos^{-1} \left[\frac{A}{J} \cos \eta \right], & \left| \frac{A}{J} \cos \eta \right| < 1 \\ 1, & \frac{A}{J} \cos \eta < -1 \end{cases} \quad (53)$$

and

$$p_l(\eta) = \begin{cases} 1, & \frac{A}{J} \sin \eta > 1 \\ 1 - \frac{1}{\pi} \cos^{-1} \left[\frac{A}{J} \sin \eta \right], & \left| \frac{A}{J} \sin \eta \right| < 1 \\ 0, & \frac{A}{J} \sin \eta < -1 \end{cases} \quad (54)$$

Again the case of most interest is $\text{SNR}_i = A^2/J^2 \ll 1$, which leads to

$$1 - 2p_u(\eta) \cong \frac{2A}{\pi J} \cos \eta \quad (55)$$

$$1 - 2p_l(\eta) \cong -\frac{2A}{\pi J} \sin \eta. \quad (56)$$

Comparing these with (47) and (48), we see that results (49) and (50) for Gaussian noise still hold, with $A/\sqrt{2\pi}\sigma$ replaced by $2A/\pi J$. Thus (50) becomes

$$\text{SNR}_o \cong \frac{L}{2} \frac{2A^2}{\pi^2 J^2} = \frac{2}{\pi^2} \left(\frac{\text{TW}}{2} \right) \text{SNR}_i. \quad (57)$$

A misleading comparison often made is between (57) and (15); this shows that a DMF performs about $10 \log_{10}(\pi^2/2) \cong 7$ dB worse when operating against incoherent constant-amplitude interference than does the corresponding analog matched filter when operating *against white noise*. The proper comparison is between the performances for the *same* type of interference. Thus, for example, (A-8) of Appendix A gives the output SNR for an analog matched filter faced with incoherent constant-amplitude interference, when the signal amplitude has a triangular correlation function⁷ and the interference has a triangular covariance function (see (A-4) and (A-5)). Using (A-8) in (14) and comparing the result with (57), one sees that the DMF performs $10 \log_{10}(3\pi^2/4) \cong 8.7$ dB worse than the corresponding analog filter for this type of interference.

As mentioned at the end of Section III, it is possible to improve the DMF's operation by optimizing the predigitizer low-pass filter in Fig. 3. For example, if incoherent interference results from a sine wave, offset from the carrier, a prefilter with a notch correspondingly offset from dc should be used. Since the specifications of the optimum prefilter depend on the interference, ideally one should use an adaptive prefilter. (In fairness, one should then also consider for comparison an analog matched filter which has an adaptive noise prewhitener [2].) As a nonadaptive compromise, a prefilter which is matched to the rectangular chip waveform is often used. For the case just considered (signal correlation and interference covariance given by (A-4) and (A-5)), such a prefilter enhances the DMF's performance by 1.7 dB.⁸ The price paid for this enhancement is that the signal waveform at the prefilter output, instead of being rectangular as for a zonal prefilter, is now composed of triangular and trapezoidal segments. In order to obtain the full 1.7 dB, the sampler must now sample precisely at the end of each incoming chip. Thus the need for chip synchronization is introduced in exchange for the 1.7-dB enhancement.

B. Constant Interference Samples

We now look at the case in which the interference samples n_{uj} and n_{ij} are random variables which stay constant from chip to chip; $n_{u1} = n_{u2} = \dots = n_{uL}$ and $n_{i1} = n_{i2} = \dots = n_{iL}$. In particular, we analyze the case of constant-amplitude coherent jamming, for which (24) and (25) become

$$n_{uj} = \frac{J}{2} \cos [\phi + \eta] \quad (58)$$

$$n_{ij} = -\frac{J}{2} \sin [\phi + \eta] \quad (59)$$

where ϕ is a uniformly distributed random variable which is independent of j . Such interference samples can originate

⁷For example, a pseudorandom code such as a maximal-length shift-register code; see [2], Figs. 16 and 17, and also footnote 11, below.

⁸This is seen by using (A-7) to obtain the prefilter's output SNR, and letting δ be the chip energy $A^2\delta/4$. The resulting SNR of $3A^2/2J^2$ is 1.7 dB higher than $\text{SNR}_i = A^2/J^2$.

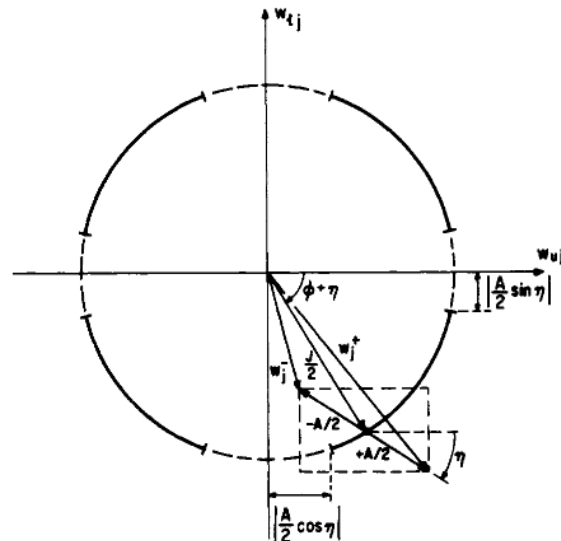


Fig. 4. Signal and interference phasors for the case of coherent constant-amplitude interference.

from a sine-wave jammer at or near the carrier frequency, which is stable enough so that its phase remains essentially constant relative to the receiver phase η over L chips but is unstable enough that its relative phase fluctuates at random from L chip transmission to L chip transmission. As we shall see, phase-shift keying ($N(t) = \pm J$) can be superimposed on this jamming without significantly changing the results we shall obtain.

We first analyze the case in which $\text{SNR}_i = A^2/J^2 \leq 1$. This situation is depicted in Fig. 4, where the phasors

$$w_j = w_j^\pm \triangleq \pm \frac{A}{2} e^{-i\eta} + \frac{J}{2} e^{-i(\phi+\eta)} \quad (60)$$

are shown ($i = \sqrt{-1}$). The real and imaginary parts of w_j are, respectively, w_{uj} and w_{ij} of (22) and (23), with $S_j = \pm A$ and n_{uj} and n_{ij} as in (58) and (59).

Notice that for the geometry shown, as the code S_1, \dots, S_L goes through its sequence of $+A$'s and $-A$'s, the resultant phasor w_j flips back and forth between w_j^+ and w_j^- but never leaves the fourth quadrant, i.e., w_{uj} and w_{ij} never change sign as j changes. For this geometry, the digitized samples are

$$w_{uj}^0 = \text{sgn} [\text{Re } w_j] = +1, \quad \text{all } j \quad (61)$$

$$w_{ij}^0 = \text{sgn} [\text{Im } w_j] = -1, \quad \text{all } j. \quad (62)$$

Supposing that the excess of the number of +1's over the number of -1's in the sequence $\{S_j^0 = \text{sgn } S_j\}$ is Q (e.g., $Q = 0$ or $Q = \pm 1$ for a pseudorandom sequence,⁹ according to whether L is even or odd), we then have, from (27) and (28),

$$\tilde{v}_{uL} = Q \quad (63)$$

$$\tilde{v}_{iL} = -Q \quad (64)$$

whence $\tilde{z} = \tilde{v}_{uL}^2 + \tilde{v}_{iL}^2 = 2Q^2$ is the DMF output at $k = L$.

For a given value of η , the result just obtained holds whenever the tip of the phasor $(J/2)e^{-i(\phi+\eta)}$ lies on one of the darkened arcs of the circle in Fig. 4. Elementary trigonometry

⁹See footnote 11.

shows that the probability that ϕ has a value which causes this to be true is

$$\alpha(\eta) = 1 - \frac{2}{\pi} \left[\sin^{-1} \left| \frac{A}{J} \sin \eta \right| + \sin^{-1} \left| \frac{A}{J} \cos \eta \right| \right]. \quad (65)$$

On the other hand, with probability $1 - \alpha(\eta)$, the tip of the phasor $(J/2)e^{-(\phi+\eta)}$ lies on the broken-line parts of the circle, in which case either

$$w_{uj}^0 \equiv +S_j^0, \quad \text{or } w_{uj}^0 \equiv -S_j^0, \quad \text{for all } j \quad (66)$$

or

$$w_{lj}^0 \equiv +S_j^0, \quad \text{or } w_{lj}^0 \equiv -S_j^0, \quad \text{for all } j. \quad (67)$$

That is, either w_{uj}^0 or w_{lj}^0 agrees perfectly with $+S_j^0$ or $-S_j^0$ for every j , the sign depending on η . It is clear from Fig. 4 that w_{uj}^0 and w_{lj}^0 cannot both perfectly agree with the digitized signal; if one does, then the other must assume a constant value of +1 or -1 for all j (cf. (61) and (62)). Hence, with probability $1 - \alpha(\eta)$, $\tilde{z} = \tilde{v}_{uL}^2 + \tilde{v}_{lL}^2 = L^2 + Q^2$.

We therefore have

$$E_S(\tilde{z}|\eta) = 2Q^2 \alpha(\eta) + (L^2 + Q^2)[1 - \alpha(\eta)] \quad (68)$$

$$E_{NS}(\tilde{z}|\eta) = 2Q^2 \quad (69)$$

$$\text{var}_S(\tilde{z}|\eta) = (L^2 - Q^2)^2 \alpha(\eta)[1 - \alpha(\eta)]. \quad (70)$$

Averaging these over η and using (40)–(42), we have

$$\text{SNR}_o = \frac{1 - \bar{\alpha}}{\bar{\alpha}} \quad (71a)$$

where

$$\bar{\alpha} = \frac{2}{\pi} \int_0^{\pi/2} \alpha(\eta) d\eta. \quad (71b)$$

Note that this result is independent of Q and would be so even if Q were to change randomly from transmission to transmission, a signalling technique to which we shall return later.

For $A/J \ll 1$, equation (65) becomes

$$\alpha(\eta) \approx 1 - \frac{2}{\pi} \left| \frac{A}{J} \right| [|\sin \eta| + |\cos \eta|] \quad (72)$$

and (71a) becomes

$$\text{SNR}_o \approx \frac{8}{\pi^2} \frac{A}{J} = \frac{8}{\pi^2} \sqrt{\text{SNR}_i}. \quad (73)$$

On the other hand, for $A/J \rightarrow 1$, $\alpha(\eta) \rightarrow 0$ and $\text{SNR}_o \rightarrow \infty$.

As noted, the results just obtained hold for $\text{SNR}_i \leq 1$. For $\text{SNR}_i = A^2/J^2 > 1$, it is impossible for both \tilde{v}_{uL} and \tilde{v}_{lL} to be reduced in magnitude from L to Q as in (63) and (64); at most, one such reduction is possible. More precisely, it can easily be shown that $\tilde{z} = L^2 + Q^2$ with probability

$$\beta = \frac{8}{\pi^2} \int_0^{\sin^{-1}|J/4|} \cos^{-1} \left[\left| \frac{A}{J} \right| \sin \gamma \right] d\gamma \quad (74)$$

and that $\tilde{z} = 2L^2$ with probability $1 - \beta$. The important point here is not the value of β but that, when the signal is present and $\text{SNR}_i > 1$, $\tilde{z} \geq L^2 + Q^2$, while when the signal is absent, $\tilde{z} = 2Q^2$. Thus except in the trivial case when $Q = L$, the DMF output at $k = L$ is always greater with the signal than without.

That is, signal detection can be achieved perfectly, a situation usually associated with $\text{SNR}_o = \infty$. On the other hand, uncritical application of (42) would lead to $\text{SNR}_o < \infty$. This is one of the cases previously discussed in which the SNR is a poor performance measure. Suffice it to say that for $\text{SNR}_i > 1$, we may take SNR_o to be effectively infinite.

The just-derived behavior of the DMF in the face of coherent constant-amplitude interference is one of capture. For $\text{SNR}_i \geq 1$, the interference cannot destroy both of the digital correlations \tilde{v}_{uL} and \tilde{v}_{lL} ; the signal in effect captures the DMF and performance is virtually perfect. For $\text{SNR}_i < 1$, the interference can totally annihilate both correlations, i.e., it can capture the DMF and performance deteriorates rapidly. To appreciate the magnitude of the deterioration, equation (73) should be compared with the corresponding result for the analog filter, which is obtained by dividing (A-13) of Appendix A by a factor of four in accordance with (14). One sees that the analog filter has a processing gain proportional to $(TW)^2$, while the DMF has no processing gain. The effect of capture by coherent constant-amplitude interference is indeed so severe that—as we shall see in Section VI—adding noise at the receiver improves the situation; this is the so-called dithering technique.

It should be noted that if an optimum predigitizing filter were used in this case, a major improvement in the DMF performance would be effected. Such a filter would have a notch at dc, which would fully reject the interference. (As noted in connection with (A-13), the extraordinary processing gain of the analog matched filter derives from a similar notch introduced by that filter at the carrier frequency.) A dc notch is therefore a worthwhile countermeasure against the possibility of unkeyed coherent interference.

A final word on coherent constant-amplitude interference is necessary, namely, that superimposition of phase-shift keying on the interference will not significantly change the results obtained for the case of a zonal prefilter. In Fig. 4, the interference phasor will now shift back and forth between the second and fourth quadrants, carrying the signal phasor with it. If $\text{SNR}_i < 1$ and if the interference phasor lies on a darkened arc, w_{uj}^0 and w_{lj}^0 will both be captured by the interference, alternating between +1 and -1 in synchronism with the interference's keying sequence. Then \tilde{v}_{uL} and \tilde{v}_{lL} will assume values $\pm Q^*$ (cf. (63) and (64)), where Q^* is the net number of agreements between the interference and signal phase-shift sequences (Q^* should be much smaller than L if the interference keying is random); then $\tilde{z} = 2(Q^*)^2$. On the other hand, if the tip of the interference phasor lies on a broken-line arc in Fig. 4, either w_{uj}^0 or w_{lj}^0 will satisfy (66) or (67), respectively, while the other will shift with the interference between +1 and -1 as before; then $\tilde{z} = L^2 + (Q^*)^2$. The net result for $\text{SNR}_i < 1$ is that (68)–(70) will hold with Q replaced by Q^* , while (71)–(73) will hold as is. Finally, if $\text{SNR}_i \geq 1$, \tilde{z} will equal $L^2 + (Q^*)^2$ with probability β of (74) and $2L^2$ with probability $1 - \beta$; so—as reasoned before— SNR_o will be effectively infinite. The use of a dc notch in the prefilter will not be as effective as in the unkeyed case and will be useless if the keying occurs at a rate approaching the chip rate.

We note in closing this section that nowhere was knowledge of the structure of the signal code—other than its length L —necessary to derive the SNR_o expressions for the DMF. Thus the expressions hold for any code sequence, whether it be fixed or randomly varying from transmission to transmission

as in the case of encrypted signalling. This invariance to code structure vanishes when a biased digitizer is considered, as in the next section.

V. BIASED THRESHOLDS

Up to this point, we have viewed the DMF as an approximation to the corresponding analog filter, the implication of (50), (57), and (73) being that a DMF need always have inferior performance. This implication becomes suspect when we recall that, except for Gaussian interference, the optimum signal processor need not be a linear device (see, e.g., [7, pp. 231, 245]). The question arises whether the DMF, viewed as a nonlinear device in its own right, can be configured so as to outperform the analog filter.

The answer is yes, as shown by the following example for the case of coherent constant-amplitude interference. For this example, we reconfigure the DMF so that the digitizer thresholds are biased to $H_u/2$ and $H_l/2$, i.e.,

$$w_{uj}^0 = \operatorname{sgn}(w_{uj} - H_u/2) \quad (75)$$

$$w_{lj}^0 = \operatorname{sgn}(w_{lj} - H_l/2). \quad (76)$$

In terms of the (w_{uj}, w_{lj}) plane of Fig. 4, the pair of thresholds is thereby moved from $(0, 0)$ to $(H_u/2, H_l/2)$. If this latter point is placed anywhere within the dashed rectangle of Fig. 4, equations (75) and (76) imply that both (66) and (67) hold simultaneously, whence z achieves the full correlation of $2L^2$. That is, when the interference is of the coherent constant-amplitude type, a simple change of thresholds can convert capture of the DMF by the interference (as in (63) and (64)) into capture by the signal. As previously discussed, SNR_o is now effectively infinite for all values of SNR_i . Clearly, the DMF now outperforms the analog filter.

Of course, this example is flawed, for it leaves two points unspecified: 1) how the DMF senses that the interference is of the coherent constant-amplitude type and 2) how the DMF manages properly to adjust H_u and H_l . In the following, we examine the question of threshold biasing more closely, particularly considering threshold adaptivity to type and strength of interference.

A. Optimal Thresholds

Coherent Constant-Amplitude Interference: As seen, for the case of coherent constant-amplitude interference, placement of the threshold pair $(H_u/2, H_l/2)$ within the rectangle

$$J \cos(\phi + \eta) - A \cos \eta < H_u < J \cos(\phi + \eta) + A \cos \eta \quad (77)$$

$$-J \sin(\phi + \eta) + A \sin \eta < H_l < -J \sin(\phi + \eta) - A \sin \eta \quad (78)$$

causes SNR_o to be effectively infinite. Thresholds outside the rectangle cause degradation of SNR_o toward that of (73). That is, the threshold ranges of (77) and (78) are optimal. In order to set these optimal thresholds, one need only observe the sequences w_{uj} and w_{lj} , $j = 1, \dots, L$, of (22) and (23) (where n_{uj} and n_{lj} are as in (58) and (59)); provided that one knows that the interference is of the unkeyed coherent constant-amplitude type, observation long enough to see only one sign change of $S_j = \pm A$ immediately establishes the optimal ranges (77) and (78).

Incoherent Constant-Amplitude Interference: Gooding [11], [12] has analyzed threshold biasing for incoherent constant-amplitude interference and has shown graphically how SNR_o

varies with threshold level. We now derive results analogous to his,¹⁰ as well as analytic results for optimal threshold levels.

At this juncture, we must for the first time specify characteristics of the signal code since, unlike the situation expressed by (29) and (30) *et seq.*, the probability of disagreement between S_j^0 and w_{uj}^0 (or w_{lj}^0) now depends on S_j^0 . The derivation of SNR_o for any fixed code sequence¹¹ is considerably more complex than the derivation heretofore. On the other hand, the case in which the code is changed randomly from transmission to transmission, by using a series of coin-flip sequences agreed upon by the transmitter and receiver, is only moderately more difficult to analyze than previous cases. We choose the latter approach here, which serves three purposes. First, it models the important case of encrypted transmissions. Second, it provides an approximation for the case of repeated transmission of a fixed random-looking code. (We discuss this approximation more fully later.) Third, it adequately shows the important feature of DMF's being illustrated here, i.e., their outperformance of the corresponding analog matched filter.

If we assume that each code sequence is obtained by coin flipping, then each S_j in a code is independently chosen and has equal probabilities of being $+A$ or $-A$. The zero-threshold analysis of (38)–(42) still holds but (31) and (37) must now be modified to read as follows.

$$\begin{aligned} p_u(\eta) = \frac{1}{2} \Pr \left[\frac{S_j}{2} \cos \eta + n_{uj} < \frac{H_u}{2} \mid S_j = +A \right] \\ + \frac{1}{2} \Pr \left[\frac{S_j}{2} \cos \eta + n_{uj} > \frac{H_u}{2} \mid S_j = -A \right] \end{aligned} \quad (79)$$

$$\begin{aligned} p_l(\eta) = \frac{1}{2} \Pr \left[-\frac{S_j}{2} \sin \eta + n_{lj} < \frac{H_l}{2} \mid S_j = +A \right] \\ + \frac{1}{2} \Pr \left[-\frac{S_j}{2} \sin \eta + n_{lj} > \frac{H_l}{2} \mid S_j = -A \right]. \end{aligned} \quad (80)$$

If we rewrite (79) as

$$p_u(\eta) = p_u(\eta, \gamma_u) = \frac{1}{2} f_1(\eta, \gamma_u) + \frac{1}{2} f_2(\eta, \gamma_u) \quad (81)$$

where $\gamma_u \triangleq H_u/J$ is the normalized threshold, we can use the statistics of n_{uj} and n_{lj} of (51) and (52) to show that

$$f_1(\eta, \gamma_u)$$

$$= \begin{cases} 1, & -\frac{A}{J} \cos \eta + \gamma_u > 1 \\ 1 - \frac{1}{\pi} \cos^{-1} \left(-\frac{A}{J} \cos \eta + \gamma_u \right), & \left| -\frac{A}{J} \cos \eta + \gamma_u \right| < 1 \\ 0, & -\frac{A}{J} \cos \eta + \gamma_u < -1 \end{cases} \quad (82)$$

¹⁰Gooding's digitizer is somewhat different than ours.

¹¹At this point, the definition of several terms to be subsequently used is worth while. "Randomly changing" or "coin-flip" codes are sequences of codes chosen by flipping a fair coin. A "fixed" code is any unchanging sequence of +1's and -1's. A "fixed random-looking" code is a fixed code which appears random to a casual observer; it may be a single coin-flip sequence or deterministically generated. A "pseudorandom" code is a fixed random-looking code which very nearly has all the statistics of the ensemble of coin-flip codes, e.g., equal numbers of +1's and -1's, equal numbers of all four sequences of two chips, etc.; maximal-length shift-register codes [14] are pseudorandom.

and

$$f_2(\eta, \gamma_u)$$

$$= \begin{cases} 0, & \frac{A}{J} \cos \eta + \gamma_u > 1 \\ \frac{1}{\pi} \cos^{-1} \left(\frac{A}{J} \cos \eta + \gamma_u \right), & \left| \frac{A}{J} \cos \eta + \gamma_u \right| < 1. \\ 1, & \frac{A}{J} \cos \eta + \gamma_u < -1 \end{cases} \quad (83)$$

Similar expressions can be written for p_l .

Gooding's results [11], [12] imply that the use of these expressions for p_u and p_l in (38)–(42) will lead to values of SNR_o which are strongly dependent on γ_u and γ_l , with a sharp maximum at an optimal threshold pair (γ_u, γ_l) . This type of behavior can be understood by examining graphs of $p_u(\eta, \gamma_u)$ and $p_l(\eta, \gamma_l)$ as functions of γ_u and γ_l , such as shown in Fig. 5. In conducting this examination, note from (38)–(42) that SNR_o depends on p_u only through $(1 - 2p_u)^2$, and it can be shown that this dependence is monotone increasing in $|1 - 2p_u|$.¹² Thus γ_u should be chosen so that $|1 - 2p_u|$ is maximized. Fig. 5 shows that the optimal value of γ_u is therefore

$$\gamma_{u,\text{opt}} = \pm \max [0, 1 - (A/J) |\cos \eta|]. \quad (84)$$

The corresponding optimal value of $|1 - 2p_u|$ is

$$|1 - 2p_u(\eta)| = \frac{1}{\pi} \cos^{-1} [1 - 2(A/J) |\cos \eta|] \quad (85)$$

where the right-hand side is taken to be unity when $(A/J) |\cos \eta| > 1$.

When $\text{SNR}_i = A^2/J^2 \ll 1$, which is the case of interest here, equation (85) can be approximated by

$$|1 - 2p_u(\eta)| \approx \frac{2}{\pi} \sqrt{(A/J) |\cos \eta|}. \quad (86)$$

A similar analysis leads to the optimal values of $\gamma_l \triangleq H_l/J$ and $p_l(\eta)$ given by

$$\gamma_{l,\text{opt}} = \pm \max [0, 1 - (A/J) |\sin \eta|] \quad (87)$$

and

$$|1 - 2p_l(\eta)| \approx \frac{2}{\pi} \sqrt{(A/J) |\sin \eta|}. \quad (88)$$

When (86) and (88) are placed into (38)–(42), one obtains for $A^2/J^2 \ll 1$

$$\text{SNR}_o \cong \frac{L(L-1)(16/\pi^3)^2 (A/J)^2}{2[(2(3-2L)+KL(L-1))(8/\pi^4)(A/J)^2 + 2(L-2)(16/\pi^3)(A/J) + 2]} \quad (89a)$$

where

$$K \triangleq 1 + \frac{2}{\pi} - \frac{16}{\pi^2} \cong 0.016. \quad (89b)$$

¹²The monotone behavior is also intuitively clear; $p_u = 1/2$ is the worst case, corresponding to the destruction of correlation, while $p_u = 0$ or 1 corresponds to full correlation. (Although $p_u = 1$ implies that $w_{uj}^0 \equiv -S_j^0$ for all j , this phase reversal is of no importance in a non-coherent DMF.)

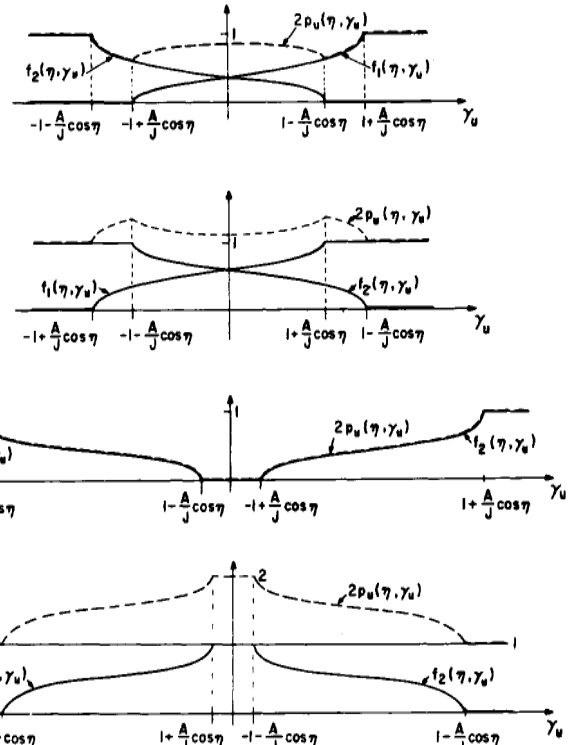


Fig. 5. Sketches of $2p_u(\eta, \gamma_u)$ as a function of γ_u . (a) $(A/J)|\cos \eta| < 1, \cos \eta > 0$. (b) $(A/J)|\cos \eta| < 1, \cos \eta < 0$. (c) $(A/J)|\cos \eta| > 1, \cos \eta > 0$. (d) $(A/J)|\cos \eta| > 1, \cos \eta < 0$.

An interesting phenomenon appears in (89a); $L \rightarrow \infty$ no longer implies $\text{SNR}_o \rightarrow \infty$ as in previous results but rather $\text{SNR}_o \rightarrow 16/\pi^2 K (\cong 20 \text{ dB})$. This is because the term containing K (which derives from the second term in (44)) dominates the denominator as $L \rightarrow \infty$, the dominance occurring for larger L , the smaller A/J is. However, since K is so small, this effect is negligible in the range of validity of (89a) for values of L up to several hundred.

For such moderate L and for the region of interest, $\text{SNR}_i \ll 1$ and $\text{SNR}_o \gg 1$, equation (89a) reduces to

$$\text{SNR}_o \cong \frac{4L}{\pi^3} \left(\frac{A}{J} \right) = \frac{8}{\pi^3} \left(\frac{\text{TW}}{2} \right) \sqrt{\text{SNR}_i}. \quad (90)$$

Comparison of (90) with (57) shows that

$$\frac{(\text{SNR}_o)_{\text{optimal}}}{(\text{SNR}_o)_{\text{zero threshold}}} \cong \frac{4}{\pi \sqrt{\text{SNR}_i}} \xrightarrow{\text{SNR}_i \rightarrow 0} \infty. \quad (91)$$

The limit in (91) implies that, over that range of $\text{SNR}_i \ll 1$ for which $\text{SNR}_o \gg 1$, use of the optimal threshold pair of

(84) and (87) can improve the DMF performance significantly over the zero-threshold case.¹³ Indeed, as in the case of coherent constant-amplitude jamming, we see that effective use of the DMF's threshold nonlinearity can make the DMF perform better even than the associated analog filter.

¹³Even in the less interesting region where $\text{SNR}_i \ll 1$ and $\text{SNR}_o \ll 1$, large improvements can be gained by the use of optimal thresholds; see Fig. 8, below.

B. Suboptimal Thresholds

A difficulty in achieving the performance of (89) and (90) is that the receiver must not only know that the interference is of the incoherent constant-amplitude type but also know the values of A/J and η in order to establish the optimal thresholds. These latter variables could be measured with elaborate enough equipment and enough time but the problem is nontrivial. A simplification is to suboptimize the threshold pair by replacing (84) and (87) by

$$\gamma_u = \gamma_l = 1. \quad (92)$$

These thresholds can be established by knowing only the value of J . Since J dominates A in the range of interest, $\text{SNR}_i \ll 1$, the value of J can be easily derived from a simple strength measurement on the total signal plus interference. (One implementation is that of digitizers with constant thresholds, fed by AGC-controlled scaling amplifiers.)

If the suboptimal thresholds of (92) are used, equations (86) and (88) become

$$|1 - 2p_u(\eta)| \cong \frac{\sqrt{2}}{\pi} \sqrt{(A/J) |\cos \eta|} \quad (93)$$

$$|1 - 2p_l(\eta)| \cong \frac{\sqrt{2}}{\pi} \sqrt{(A/J) |\sin \eta|} \quad (94)$$

which leads to the replacement of (90) by

$$\text{SNR}_o \cong \frac{4}{\pi^3} \left(\frac{\text{TW}}{2} \right) \sqrt{\text{SNR}_i} \quad (95)$$

i.e., a 3-dB deterioration in SNR_o (6 dB in SNR_i) from optimum. This is not much of a price to pay for the simplicity of threshold setting achieved. The transition from (90) to (95) does show, however, the extreme sensitivity of SNR_o to the threshold level. For example, if $\text{SNR}_i = -20$ dB, then going from optimal thresholds to those of (92) involves less than a 10-percent change in the threshold level but is accompanied by a 50-percent decrease in SNR_o . If $\text{SNR}_i = -30$ dB, less than a 3-percent change in the threshold level leads to a 50-percent decrease in SNR_o . This sensitivity has been noted also by Gooding [11], [12]. It stems from the necessity of setting the threshold at a level where the digitizer is controlled by the signal; the smaller the signal is compared to the interference, the more critical this setting will be.

C. Remarks on Optimal and Suboptimal Thresholds

As indicated earlier in this section, the results just obtained for randomly chosen codes provide approximations for the case of a fixed random-looking code. These approximations are in fact lower bounds, because randomly changing codes can cause additional variation in the correlation variable \tilde{z} from transmission to transmission, thus increasing the variance of \tilde{z} and decreasing SNR_o . The amount of degradation depends critically on the threshold level, vanishing for zero threshold (see the last paragraph of Section IV) and becoming large for the optimal and suboptimal thresholds defined above (see Section VII). The degradation also depends on L , vanishing as $L \rightarrow \infty$, when all coin-flip codes look statistically much alike and are well approximated by a fixed pseudorandom code.

The difficulty with trying to work at or near optimal threshold levels is clear from preceding discussions. First, the receiver must be able to determine the type of interference. Second, it must set threshold levels on the basis of certain

measured parameters peculiar to that type of interference, using, e.g., (77) and (78) for the coherent constant-amplitude case or (84) and (87) for the incoherent constant-amplitude case (or, as is easily shown, zero thresholds for the Gaussian case). Finally, assuming that the threshold levels are properly set, they must be adaptively maintained within extremely severe tolerances, which generally become more severe as $\text{SNR}_i \rightarrow 0$. The tolerance problem is compounded by the fact that the measurement of threshold-setting parameters also becomes more difficult as $\text{SNR}_i \rightarrow 0$.

D. Nonparametric Adaptive Thresholds

Clearly, it is necessary to establish threshold levels which are nonparametric, i.e., work well—although not optimally—individually of the type of interference which occurs. Further, these should be adaptive in the closed-loop sense; that is, instead of being set by predigitizer measurements which depend on the type of interference, the thresholds should be set by postdigitizer measurements which depend only on digitizer performance. Such a feedback technique will allow the thresholds to respond adaptively to deteriorating performance, independently of the type or strength of the interference.

One such nonparametric closed-loop scheme involves keeping constant the fraction of +1's emitted from the digitizer.¹⁴ If the fraction of +1's becomes too large, a feed-back signal increases the threshold and reduces the fraction of +1's; the reverse action occurs when the fraction of +1's becomes too small. This technique can be easily implemented by use of an RC integrator following the digitizer, the output of which biases the digitizer.

The philosophy behind the technique just described is one of preventing capture by the interference. For example, suppose strong coherent constant-amplitude interference of the form in (60) is present with $A^2/J^2 \ll 1$ and the feedback is set for 50 percent +1's. Then the thresholds will automatically settle into the optimal ranges given by (77) and (78) and the determination of whether the digitizer output is +1 or -1 will depend solely on the signal. The optimal-threshold behavior described in the previous subsection will hold.

The best feedback bias setting will depend on the type of interference. The "50 percent +1's" setting just discussed will obviously lead to near-zero thresholds for incoherent constant-amplitude interference when $A^2/J^2 \ll 1$, and the digitizer outputs will be almost completely determined by the interference rather than the signal. A compromise setting which seems to be acceptable for various types of interference is 25 percent +1's, and it is this value which we shall adopt in our analysis.

Coherent Constant-Amplitude Interference: When the interference is of the coherent constant-amplitude type given by (60), feedback set for 25 percent +1's will cause the thresholds ($H_u/2, H_l/2$) to settle at the upper right-hand corner of the rectangle in Fig. 4. Digitizer behavior for this threshold location at first seems indeterminate, since slight displacements of H_u or H_l cause abrupt changes from 50 to 0 percent +1's in the associated digitizer output. However, if one hypothesizes a slight amount of zero-median ambient noise at each digitizer input, this indeterminacy vanishes; the ambient noise vector, added to w_j of (60), will cause the resultant vector to lie to the

¹⁴This technique was called to the author's attention by personnel at Hughes Aircraft Company.

right of the rectangle 25 percent of the time and above the rectangle 25 percent of the time.

In order to find SNR_o , consider the correlation

$$\tilde{v}_{uL} = \sum_{j=1}^L S_j^0 w_{uj}^0 \quad (96)$$

and suppose, for illustration, that exactly one-half of the S_j^0 's are +1 and the other half are -1. Examination of Fig. 4 shows that when $H_u/2$ is positioned as indicated above, S_j^0 and w_{uj}^0 will agree for all $L/2$ j's for which $S_j^0 = -1$ (and hence $w_j = w_j^0$). For the other $L/2$ j's, S_j^0 and w_{uj}^0 will agree only with probability 1/2, because of the ambient noise. If the noise is independent from chip to chip, \tilde{v}_{uL} can therefore be modeled as a constant, $L/2$, plus a sum with $L/2$ independent terms which are +1 or -1, each with probability 1/2. The application of (34) and (36) then leads to

$$E_S[\tilde{v}_{uL}^2] = (L/2)^2 + L/2 \quad (97)$$

$$\text{var}_S[\tilde{v}_{uL}^2] = L(L/2 - 1). \quad (98)$$

On the other hand, when no signal is present, H_u will move to a position in which the ambient noise plus the constant-amplitude interference will cause a random 25 percent of the w_{uj}^0 's to be +1. The probability of any w_{uj}^0 agreeing with S_j^0 will be 1/2, and \tilde{v}_{uL} will be a sum of L independent terms which are +1 or -1, each with probability 1/2. Then

$$E_{NS}[\tilde{v}_{uL}^2] = L. \quad (99)$$

Identical results hold for \tilde{v}_{IL} , whence—assuming independence of the ambient noise components in the w_{uj} and w_{ij} directions—equation (42) leads to

$$\text{SNR}_o = L \left(\frac{L}{2} - 1 \right) \cong \frac{L^2}{2} = \frac{(\text{TW})^2}{2} \quad (100)$$

for the case of codes having exactly one-half +1's. Note that even though SNR_o is no longer effectively infinite as in the case of optimal thresholds, it is still very large and virtually independent of SNR_i .¹⁵ SNR_o of (100) should be compared with SNR_o for the analog filter, i.e., (A-13) of Appendix A, divided by a factor of four in accordance with (14); again we see the possibility of outperforming the analog filter with a DMF.

Incoherent Constant-Amplitude Interference: For IID interference, feedback set for 25 percent +1's requires that H_u satisfy

$$\begin{aligned} \Pr[+1 \text{ out}] &= \frac{1}{2} \Pr \left[\frac{S_j}{2} \cos \eta + n_{uj} > \frac{H_u}{2} \mid S_j = +A \right] \\ &+ \frac{1}{2} \Pr \left[\frac{S_j}{2} \cos \eta + n_{uj} > \frac{H_u}{2} \mid S_j = -A \right] = 0.25 \quad (101a) \end{aligned}$$

for all j . (Here we have again assumed randomly chosen coin-flip codes for simplicity.) For $\text{SNR}_i \ll 1$, equation (101a)

becomes approximately

$$\Pr \left[n_{uj} > \frac{H_u}{2} \right] \cong 0.25. \quad (101b)$$

When the n_{uj} are as in (51), it is clear that an approximate solution to (101b) is $\gamma_u = H_u/J \cong 1/\sqrt{2}$. Using this value of γ_u in (81)–(83) and using only through the first-power term in a Taylor series around $1/\sqrt{2}$ to approximate the inverse cosines, one obtains

$$|1 - 2p_u(\eta)| = \frac{2\sqrt{2}}{\pi} \frac{A}{J} |\cos \eta|. \quad (102)$$

Similarly, one can show that

$$|1 - 2p_l(\eta)| = \frac{2\sqrt{2}}{\pi} \frac{A}{J} |\sin \eta|. \quad (103)$$

A comparison of (102) and (103) with (55) and (56) shows that (57) is replaced by

$$\text{SNR}_o = \frac{4}{\pi^2} \left(\frac{\text{TW}}{\pi} \right) \text{SNR}_i. \quad (104)$$

That is, use of "25 percent +1's" thresholds improves performance by 3 dB over use of zero thresholds. While this performance does not exceed that of the analog filter and is even further from the optimal-threshold performance of (91), it is an improvement which cannot be ignored considering the ease with which the adaptive thresholds can be implemented. In line with our previous comments on the difference between random and fixed coding, we note here that simulation results presented in Section VII show virtually no change from (104) when a pseudorandom code is used. That is, at the adaptive threshold level of $1/\sqrt{2}$, the degradation suffered by going to random coding from pseudorandom coding is negligible.

Gaussian Noise: In order to determine the performance of "25 percent +1's" thresholds when the interference is Gaussian noise, we solve (101b) for H_u when n_{uj} is Gaussian with variance $\sigma^2 = N_0 W/4$ (see Appendix E). Assuming that $A/\sigma \ll 1$, we obtain

$$\frac{H_u}{2} = \frac{H_l}{2} \cong 0.675\sigma \quad (105)$$

whence

$$|1 - 2p_u(\eta)| \cong 0.318 \frac{A}{\sigma} |\cos \eta| \quad (106)$$

$$|1 - 2p_l(\eta)| \cong 0.318 \frac{A}{\sigma} |\sin \eta|. \quad (107)$$

A comparison with (47) and (48), noting that $1/\sqrt{2\pi} \cong 0.4$, shows a loss of $20 \log_{10} (0.4/0.318) \cong 2$ dB compared to the zero threshold case, i.e., instead of (50), we have

$$\text{SNR}_o \cong 0.4 (\text{TW}/2) \text{SNR}_i. \quad (108)$$

We note that in these analyses of the performance of adaptive thresholds, we have assumed perfect adaptivity, i.e., a constant fraction of +1's at the digitizer outputs. Thus the effects of threshold fluctuations due to the finite averaging time of the bias circuitry and to transient changes in interference conditions have not been considered. In fact, if the

¹⁵Of course, we must have $\text{SNR}_o \rightarrow 0$ as $\text{SNR}_i \rightarrow 0$. Contrary to the implication of our previous assumption that the ambient noise is small compared to A , when $\text{SNR}_i \rightarrow 0$, we can no longer guarantee that the ambient noise will not cause disagreement between S_j^0 and w_{uj}^0 for $S_j^0 = -1$ in Fig. 4.

interference is malevolent, it can no doubt be fashioned so as to cause the thresholds constantly to hunt for equilibrium positions. Nonetheless, it is clear that threshold adaptivity is a powerful technique for improving DMF performance. Another technique is dithering, discussed in the following section.

VI. DITHERING

Consider the $w_{uj} = \operatorname{Re} w_j$ component of (60);

$$w_{uj} = \frac{S_j}{2} \cos \eta + \frac{J}{2} \cos(\phi + \eta) \quad (109)$$

where $S_j = \pm A$. An example of this sequence is shown by the solid circles in Fig. 6, for a case in which $\operatorname{SNR}_o = A^2/J^2 < 1$. Notice that if the threshold is set at zero, as in Section IV, $w_{uj}^0 = +1$ for all j and the \tilde{v}_{uL} correlation is destroyed. One method of restoring correlation, as discussed in Section V, is to move the threshold so that it lies between the broken lines in Fig. 6 (see (77)). Another is to "dither" either the threshold or the w_{uj} 's by the use of noise, as follows.

Suppose noise samples d_{uj} are added to the w_{uj} above. The values of $w_{uj} + d_{uj}$ are shown in Fig. 6 by open circles. Notice that for the d_{uj} sequence chosen, $w_{uj} + d_{uj} < 0$ for $j = 3$ and 8 and these chips are emitted from the zero-threshold digitizer as $w_{uj}^0 = -1$. Thus partial correlation is restored by the addition of noise at the receiver. In essence, dithering allows the receiver to seize partial control of the interference so as to make it less destructive of correlation than is the channel's interference. Clearly, the statistics of the dither samples d_{uj} should be such that the w_{uj} 's on the lower level in Fig. 6 are moved below threshold with high probability, while the w_{uj} 's on the upper level are almost never shifted that far. This requires control of the dither statistics by circuitry that measures these two levels.

It is seen that, equivalently, the w_{uj} 's can be left as is and the threshold dithered by amount $-d_{uj}$. One may ask why this random biasing of the threshold should be used when a constant threshold bias can achieve much more, at least in the case of the coherent constant-amplitude interference shown in Fig. 6. A partial answer is that if the interference is malevolently controlled jamming, the jammer is in theory capable of successfully attacking any deterministic threshold-biasing scheme. The receiver's defense is to choose a random threshold strategy. We thus have a game-theoretical situation governed by minimax principles; the jammer tries to choose interference so as to minimize SNR_o , while the receiver chooses dither so as to maximize it.

Cahn [4] has examined this problem. Although he analyzes a coherent DMF, his results carry over to a noncoherent DMF for large SNR_o by virtue of the argument of (13) *et seq.* Further, although Cahn assumes IID interference samples, his results also apply to coherent interference, at least when the coding is random, for then the terms in (96) (and a like expression for \tilde{v}_{uL}) are still IID.

Cahn finds that the minimaxing dither has probability density

$$g(d) = \begin{cases} \frac{\sqrt{3}}{4\sigma} \left(1 - \frac{d^2}{3\sigma^2}\right), & |d| \leq \sqrt{3}\sigma \\ 0, & \text{elsewhere} \end{cases} \quad (110)$$

where σ^2 is the variance of the channel interference as it

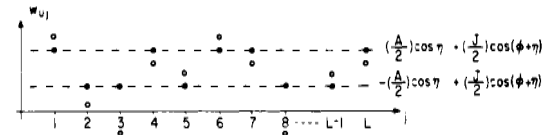


Fig. 6. Illustration of dithering for the case of coherent constant-amplitude interference.

appears at the digitizer input. When $\operatorname{SNR}_o \ll 1$, and if the dither samples are chosen independently according to this distribution, Cahn shows that there is no channel interference which can cause a coherent DMF to perform more than 4.8 dB worse than the performance specified by (6).

It has been conjectured¹⁶ that the IID dither samples postulated by Cahn are suboptimal. The intuitive reasoning behind this conjecture is as follows. The shift-register correlators act very much like the low-pass matched filters of Fig. 1. If the signal amplitude $S(\cdot)$ of (9) has an approximately triangular correlation function, the correlators will therefore have "transfer functions" with spectral nulls at multiples of the chip rate. (See (B-9) of Appendix B.) Provided that the dither spectrum can be concentrated near these nulls, the correlator will then not see the dither. That is, the dither will exert its control on the digitizer and—having served its purpose—will be suppressed by the correlator. Since IID dither has a more-or-less flat spectrum, the substance of the conjecture is that some form of dither which is dependent from chip to chip will be more efficient.

One possible dither having a nonuniform spectrum is that generated by sampling a sawtooth wave having a period of $(L-1)\delta/L$, where δ is the duration of a chip and L is the number of chips in the signal code. The dither samples are taken once per chip (i.e., every δ) so that, over one signal sequence of $L\delta$, the L dither samples are uniformly distributed over the range of the sawtooth amplitude. The dither samples are passed through a nonlinear device which shapes their distribution to that given by (110). In the next section, we shall show simulation results which tend to support the conjecture that such dither is better than IID dither.

VII. DISCUSSION OF RESULTS

In previous sections, we have made a number of comparisons between analog and digital matched-filter performances by comparing straight-line approximations to the SNR curves, e.g., equation (15) and (50) in the case of Gaussian interference. These comparisons were heuristically valuable but have limited ranges of validity. In the present section, we compare the more accurate curvilinear SNR expressions, which have wider ranges of validity. We also present the results of computer simulations of DMF's, which verify the accuracy of the curvilinear expressions.¹⁷

In all results given below, $L = \text{TW}$. Many of the simulation results are taken from [13].

¹⁶Source of conjecture unknown.

¹⁷All simulations were run by using repeated trials (transmissions) and estimating the terms in (42) by corresponding sample averages. Trials were continued by increasing their number 50 percent at a time until the estimated SNR_o varied less than 0.5 dB from one step in the procedure to the next. Several hundred trials usually resulted for each simulation point.

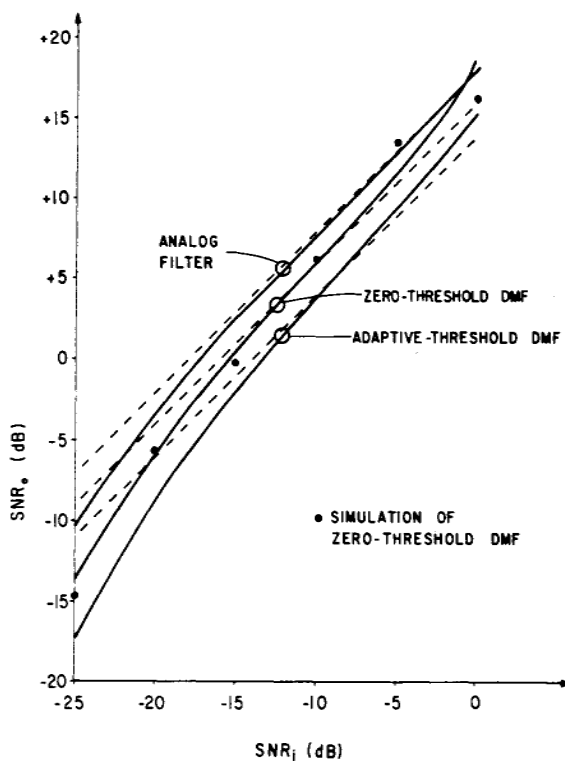


Fig. 7. SNR curves: white Gaussian interference ($L = 127$).

A. Gaussian Interference

When the channel interference is Gaussian, the analog square-law matched filter is governed by (C-11), with $k = 4$ and $\text{SNR}_o(y_e)$ given by (6). That is,

$$\text{SNR}_o = \frac{L^2(\text{SNR}_i)^2}{2L(\text{SNR}_i) + 1}. \quad (111)$$

The corresponding performance of the zero-threshold DMF is given by (49), with SNR_i as in (46), i.e.,

$$\text{SNR}_o = \frac{(4/\pi^2)L(L-1)(\text{SNR}_i)^2}{(3/\pi^2)(3-2L)(\text{SNR}_i)^2 + (4/\pi)(L-2)(\text{SNR}_i) + 1}. \quad (112)$$

Finally, as indicated in the discussion after (106) and (107), the SNR expression for a DMF whose threshold is set adaptively to achieve 25 percent +1's is obtained by replacing SNR_i in (112) by $(0.4/0.318)^2(\text{SNR}_i) = 1.58(\text{SNR}_i)$, i.e., shifting the curve of (112) to the right by 2 dB. This latter result holds strictly for randomly changing codes but is a good approximation for a fixed random-looking code.

The three curves just described are shown in Fig. 7 for $L = 127$. The corresponding straight-line approximations (e.g., (15) and (50)) are also shown, as broken lines. One sees that

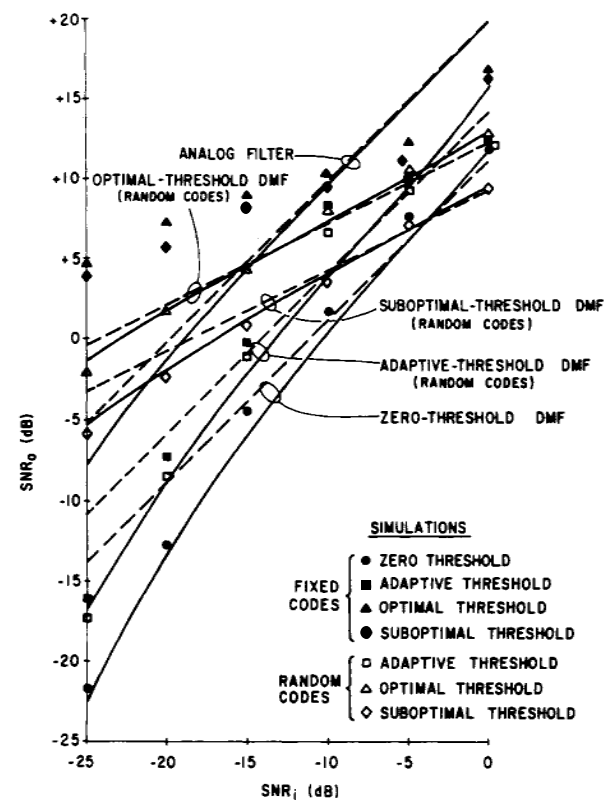


Fig. 8. SNR curves: incoherent constant-amplitude interference ($L = 127$).

in Fig. 7. These show that (112) is extremely accurate when SNR_i is less than -10 dB, and is within 1 dB almost up to $\text{SNR}_i = 1$ (0 dB).

B. Incoherent Constant-Amplitude Interference

For incoherent constant-amplitude interference and for a fixed random-looking code, the analog square-law matched filter is governed by (C-11), with $k = 4$ and $\text{SNR}_o(y_e)$ given by (A-8). That is,

$$\text{SNR}_o = \frac{9L^2(\text{SNR}_i)^2}{12L(\text{SNR}_i) + 4}. \quad (113)$$

As indicated by the discussion following (55) and (56), the zero-threshold DMF performs according to (49) for any code, with $A/\sqrt{2\pi}\sigma$ replaced by $2A/\pi J$ and $\text{SNR}_i = A^2/J^2$, i.e.,

$$\text{SNR}_o = \frac{(4/\pi^4)L(L-1)(\text{SNR}_i)^2}{(3/\pi^4)(3-2L)(\text{SNR}_i)^2 + (4/\pi^2)(L-2)(\text{SNR}_i) + 1}. \quad (114)$$

With the optimal thresholds of (84) and (87), and for randomly changing codes, the DMF is governed by (89a) with $A^2/J^2 = \text{SNR}_i$.

$$\text{SNR}_o = \frac{(64/\pi^6)L(L-1)(\text{SNR}_i)}{(4/\pi^4)[2(3-2L)+KL(L-1)](\text{SNR}_i)+(16/\pi^3)(L-2)\sqrt{\text{SNR}_i+1}}. \quad (115)$$

the straight-line approximations fit well where they are supposed to: $\text{SNR}_o \gg 1$ for the analog filter and $\text{SNR}_i \ll 1$ and $\text{SNR}_o \gg 1$ for the DMF. However, outside of these ranges, the straight-line approximations fail by substantial margins.

Simulation results for the zero-threshold DMF are also given

Use of the suboptimal thresholds of (92) causes a shift of (115) to the right by 6 dB in SNR_i (see (93) and (94) *et seq.*), while use of "25 percent +1's" adaptive thresholds causes a shift of (114) to the left by 3 dB in SNR_i (see (102) and (103) *et seq.*).

The five curves just described are shown in Fig. 8 for $L = 127$, together with corresponding straight-line approximations (e.g., (57), (90), (95), (104)). Again it is clear that the straight-line approximations fail by wide margins outside of their ranges of validity. (Of course, as is to be expected, the more exact curvilinear expressions also begin to fail in the neighborhood of $\text{SNR}_i = 0 \text{ dB}$, e.g., note that the adaptive-threshold curve exceeds the optimal-threshold curve in this region, clearly an impossibility.)

As previously noted, use of the optimal or suboptimal biased thresholds of (84), (87), and (92) substantially improves the DMF performance over the zero-threshold case, and even over the analog-filter case when SNR_i is small enough. Likewise, adaptive "25 percent +1's" thresholds lead to a nontrivial increase in SNR_o over the zero-threshold case.

The results of simulations are also shown in Fig. 8. The fixed-code simulations were run using a fixed 127-chip maximal-length shift-register (pseudorandom) sequence. The random-code simulations were run by generating a new 127-chip coin-flip sequence for each trial. Only the fixed-code simulation was run in the zero-threshold case, since the theory shows that there is no difference between fixed- and random-code performance in this case.

The match between theory and simulation is excellent almost everywhere, with two minor discrepancies. First, the simulation results for the zero-threshold case are about 1 dB higher than theory, the discrepancy no doubt arising from the slight dependence among noise variates neglected in the analysis (see Appendix E); taking these dependences into account would have decreased the variance of the correlation variable \bar{Z} , thus increasing SNR_o . A second discrepancy is apparent in the region $A/J > 1 - (1/\sqrt{2}) \cong -10 \text{ dB}$ for the adaptive-threshold case. This is just the region where the straight-line approximation to $\cos^{-1}x$ used in deriving the theoretical curve (see (101) *et seq.*) totally fails. It is noteworthy that in this region the simulation results more closely agree with the optimal-threshold curve, an agreement which can be explained by realizing that the optimal threshold of (84) is close to the adaptive-threshold value of $1/\sqrt{2}$ for $A/J \geq 1 - (1/\sqrt{2})$.

As previously noted, randomly chosen codes and fixed codes perform identically for the zero-threshold case. The simulation results of Fig. 8 show that their performances differ by the order of only 1 dB in the adaptive case, where the threshold level is set at $1/\sqrt{2}$. In the neighborhood of the thresholds of (84) and (87),¹⁸ the performances differ substantially. This is because—as previously discussed—optimal thresholds allow the signal rather than the interference to control the DMF. In the random-code case, a major contribution to the denominator of (42) will therefore result from the fluctuation of the signal structure, a term not present in the fixed-code case. Further simulations have shown the discrepancy between random- and fixed-code performances to decrease slowly as $L \rightarrow \infty$, as all randomly chosen codes begin to look statistically like a single pseudorandom code.

C. Coherent Constant-Amplitude Interference

For unkeyed coherent constant-amplitude interference (i.e., sine-wave interference near the carrier frequency) and for fixed random-looking codes, analog-filter performance follows

¹⁸These may not be optimal in the fixed-code case, but are certainly near optimal.

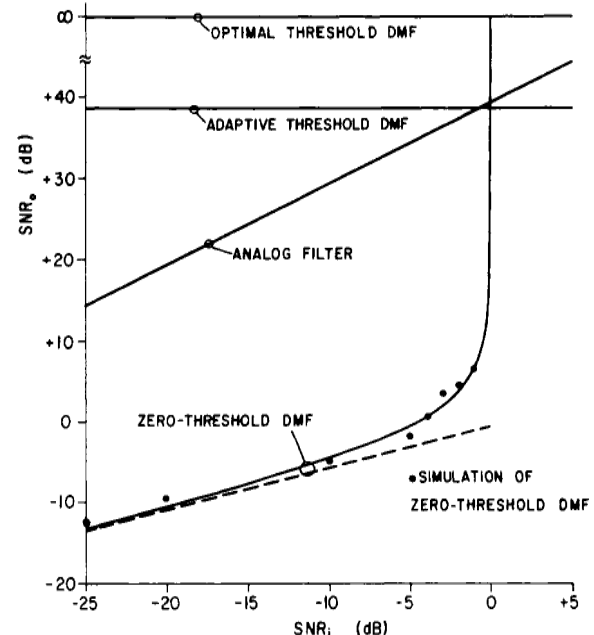


Fig. 9. SNR curves: coherent constant-amplitude interference ($L = 127$).

(C-11), with $k = 3$ and $\text{SNR}_o(y_e)$ given by (A-13). That is,

$$\text{SNR}_o = \frac{4(L/Q)^4(\text{SNR}_i)^2}{8(L/Q)^2(\text{SNR}_i) + 3} \quad (116)$$

where it is recalled that Q is the difference between the numbers of +1's and -1's in the signal sequence. For $\text{SNR}_i < 1$, the zero-threshold DMF performs according to

$$\text{SNR}_o = \frac{1 - \bar{\alpha}}{\bar{\alpha}} \quad (117)$$

independently of Q , where $\bar{\alpha}$ is given by (71b); while for $\text{SNR}_i \geq 1$, SNR_o is effectively infinite. With the optimal thresholds of (77) and (78), one effectively has

$$\text{SNR}_o = \infty \quad (118)$$

for all SNR_i , for any Q . For fixed codes with $Q = 0$, the use of "25 percent +1's" thresholds leads to (cf. (100))

$$\text{SNR}_o = L \left(\frac{L}{2} - 1 \right) \quad (119)$$

for all SNR_i for which the ambient noise is negligible (see footnote 15).

These results are shown in Fig. 9, together with the straight-line approximation of (73), for $L = 127$ and $Q = 1$ (as in a pseudorandom code). Also shown in Fig. 9 is the result of simulation of the zero-threshold DMF, showing that the theoretical expression (117) is extremely accurate.

D. Multiple Interferences

When more than one type of interference is present at once, theoretical analysis becomes difficult. Fig. 10 shows the results of fixed-code zero-threshold simulations when both Gaussian and coherent constant-amplitude interferences are simultaneously present. In the figure, the zero-threshold curve of Fig. 7 for Gaussian interference only and the zero-threshold curve of Fig. 9 for coherent constant-amplitude interference only are both shown for reference. The four other solid curves

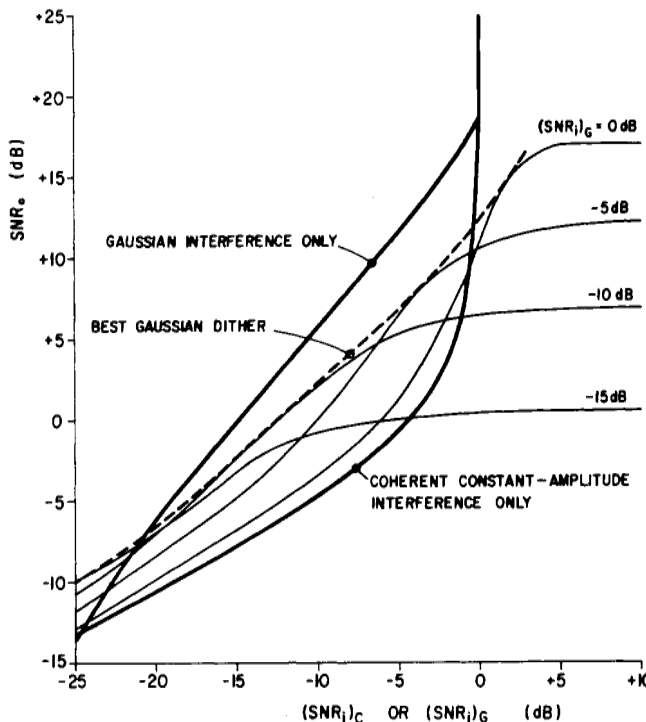


Fig. 10. SNR curves: simultaneous white Gaussian and coherent constant-amplitude interference ($L = 127$).

are smoothed simulation curves for the case when both interferences are present. For these latter curves, the abscissa is $(SNR_i)_C$, the ratio of input signal power to constant-amplitude interference power. The curves are parametrized by $(SNR_i)_G$, the ratio of input signal power to Gaussian interference power.

As previously noted and again seen in Fig. 10, the addition of noise to the coherent constant-amplitude interference in the channel actually *increases* SNR_o . In fact, as noted in Section VI, if the additional noise were not already present in the channel, it would be desirable to introduce it into the receiver as dither. The curves of Fig. 10 determine the optimal amount of Gaussian dither that should be added, as a function of $(SNR_i)_C$, so as to maximize SNR_o . The maximum SNR_o so obtained is shown by the broken-line curve, which will be compared below to Cahn's results.

E. Dither

In Fig. 11, we show for reference the zero-threshold curves for Gaussian interference and for incoherent constant-amplitude interference, taken from Figs. 7 and 8. The broken-line curve is Cahn's pessimum, as applied to a square-law matched filter. (The latter curve is the analog filter curve of Fig. 7 shifted to the right by 4.8 dB; it will be recalled that Cahn's analysis claims that no IID interference can reduce SNR_o below this pessimum when the optimal random dither specified by (110) is used.)

Also shown in Fig. 11 are the results of simulations using Cahn's optimal dither, for the two types of interference considered there. (A fixed maximal-length shift-register sequence was used for the code.) It is seen that except for very small SNR_i and for $SNR_i \approx 1$ (in which case Cahn's analysis is very approximate), the pessimum not only is a lower bound but also approximates actual performance. (See also Cahn's simulation curves in [14].)

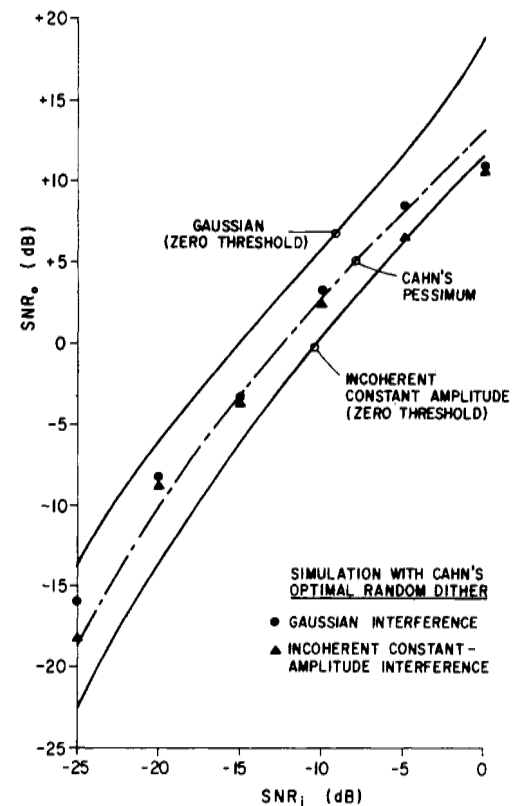


Fig. 11. Effect of dither: white Gaussian interference and incoherent constant-amplitude interference.

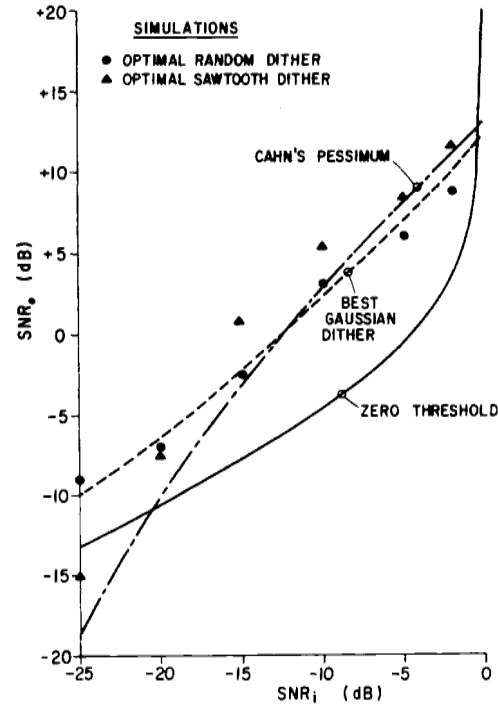


Fig. 12. Effect of dither: coherent constant-amplitude interference.

In Fig. 12, similar results are given for the case of coherent constant-amplitude interference. Shown there are the zero-threshold curve of Fig. 9, Cahn's pessimum, and the "best Gaussian dither" curve of Fig. 10. The circular dots are the

simulation results when Cahn's optimal random dither is used. One sees that these results are virtually the same as those obtained with the best Gaussian dither, i.e., the exact shape of the dither distribution seems not to be as important as the proper adjustment of the dither variance for maximum SNR_o .

The triangular dots in Fig. 12 are the simulation results when the dither is generated by periodically sampling, at the chip rate, a sawtooth wave having a period of 126/127 of the chip period, as described at the end of Section VI. This dither turns out to be consistently 2-3 dB better than random dither for SNR_i greater than -20 dB, thus lending credence to the conjecture given in Section VI, at least in the case of coherent constant-amplitude interference. On the other hand, no such advantage of sawtooth over random dither was detected in simulations for the case of incoherent constant-amplitude interference.

CONCLUSIONS

We have seen that, except in the case when only Gaussian interference is present, it is desirable to design the DMF as a device in its own right, rather than as an approximation to the analog filter. Threshold biasing and dithering are fruitful DMF design modifications. A comparison of Fig. 8 with Fig. 11 and of Fig. 9 with Fig. 12 shows that threshold biasing has an advantage over dithering, at least for the types of interference considered in those figures.

APPENDIX A EVALUATION OF EQUATION (4)

The simplest case of (4) is that of white noise, $\hat{N}(f) \equiv N_o/2$. Then, since by Parseval's theorem

$$\int_{-\infty}^{\infty} |\hat{S}(f)|^2 df \equiv \int_0^T s^2(t) dt = \mathcal{E} \quad (\text{A-1})$$

we have

$$\text{SNR}_o = 2\mathcal{E}/N_o. \quad (\text{A-2})$$

Defining $\text{SNR}_i \triangleq P_i/N_i$ and letting P_i and N_i be as in (7) and (8), one easily obtains

$$\text{SNR}_o = 2\text{TW}(\text{SNR}_i). \quad (\text{A-3})$$

Note that (A-2) and (A-3) are independent of the signal spectrum $|\hat{S}(\cdot)|^2$.

Next, suppose that $s(\cdot)$ is a fixed random-looking binary signal and that $n(\cdot)$ is incoherent constant-amplitude interference. That is, let $s(\cdot)$ have the form of (9) with $\theta(t) \equiv 0$ and $S(t) = \pm A$, where $S(\cdot)$ is allowed to change sign every δ s in a random-looking manner; and let $n(\cdot)$ have the form of (10), where $|N(t)| \equiv J$ and $\phi(\cdot)$ is a low-pass stationary random process with a bandwidth of the order of $1/\delta$. Suppose also that the autocorrelation function of $s(\cdot)$ has a perfectly triangular mainlobe [2, Figs. 17 and 18],

$$r(\tau) \triangleq \int_0^T s(t)s(t-\tau) dt = \mathcal{E} \left(1 - \frac{|\tau|}{\delta}\right) \cos \omega_0 \tau, \quad |\tau| \leq \delta \quad (\text{A-4})$$

and that the covariance function of the interference also has

approximately a triangular shape

$$k(\tau) \triangleq E[n(t)n(t-\tau)] = \begin{cases} \frac{J^2}{2} \left(1 - \frac{|\tau|}{\delta}\right) \cos \omega_0 \tau, & |\tau| \leq \delta \\ 0, & |\tau| > \delta. \end{cases} \quad (\text{A-5})$$

(The latter will hold exactly if $\phi(\cdot)$ in (10) stays constant over δ -s intervals and changes randomly from interval to interval.) Then, since $r(\cdot)$ and $k(\cdot)$ are the inverse Fourier transforms of $|\hat{S}(\cdot)|^2$ and $\hat{N}(\cdot)$, respectively, the denominator of (4) becomes

$$\int_{-\infty}^{\infty} \hat{N}(f) |\hat{S}(f)|^2 df = \int_{-\infty}^{\infty} k(\tau) r(\tau) d\tau = \frac{J^2 \mathcal{E} \delta}{6}. \quad (\text{A-6})$$

Thus (4) becomes

$$\text{SNR}_o = 6\mathcal{E}/J^2 \delta. \quad (\text{A-7})$$

Using (7), noting that $N_i \triangleq E[n^2(t)] = J^2/2$, and using the noise bandwidth $W = 1/\delta$ derived in Appendix B, we can reduce (A-7) to

$$\text{SNR}_o \cong 3\text{TW}(\text{SNR}_i). \quad (\text{A-8})$$

We note that, although (A-3) and (A-8) seem to imply that matched filtering is more effective against incoherent constant-amplitude interference than against white noise, this conclusion is not necessarily valid because of the different definitions of SNR_i in the two expressions. In (A-8), SNR_i is defined in terms of the total input interference power; in (A-3), SNR_i is defined in terms of only that input noise power contained in W Hz of bandwidth. (The total input noise power in the latter case is infinite.) The value of (A-3) and (A-8) lies not in a comparison between them but in the comparison of each with a corresponding expression for DMF performance with the same type of interference.

For a final evaluation of (4), consider the case of coherent constant-amplitude interference, i.e.,

$$n(t) = J \cos(\omega_i t + \phi). \quad (\text{A-9})$$

Here, ϕ is a random variable and J and ϕ are assumed constant, at least over the interval $0 \leq t \leq T$ of signal transmission. $\hat{N}(f)$ now consists of delta functions of area $J^2/2$ at $f = \pm \omega_i/2\pi$, and (4) becomes

$$\text{SNR}_o = \frac{2\mathcal{E}}{J^2 |\hat{S}(f_i)|^2}. \quad (\text{A-10})$$

A case of interest is when $f_i = f_0 = \omega_0/2\pi$ (the carrier frequency) and $s(\cdot)$ is a phase-shift-keyed binary signal. Then, using (9) with $\theta(t) \equiv 0$ and $S(t) = \pm A$ holding constant over δ -s intervals,

$$\begin{aligned} \hat{S}(f_0) &\triangleq \int_{-\infty}^{\infty} S(t) \cos \omega_0 t \exp(-j\omega_0 t) dt \\ &\cong \frac{A}{2} Q \delta \end{aligned} \quad (\text{A-11})$$

where Q is the excess of the number of $+A$'s over the number of $-A$'s in the keying sequence. ($Q = 0$ or $Q = \pm 1$ for a pseudo-random sequence, according to whether the sequence is of

even or odd length.) Then (A-10) becomes

$$\text{SNR}_o = \frac{8\delta^2}{J^2 A^2 Q^2 \delta^2}. \quad (\text{A-12})$$

Use of (9) in (5) with $S(t) = \pm A$ leads to $\delta = A^2 T/2$, whence (7) yields $P_i = A^2/2$. These results, together with $N_i = J^2/2$ and $W = 1/\delta$, allow (A-12) to be written as

$$\text{SNR}_o = 2 \frac{(TW)^2}{Q^2} (\text{SNR}_i). \quad (\text{A-13})$$

Notice that when $Q = 0$, $\text{SNR} = \infty$, which reflects the fact that the notch in the matched-filter transfer function at f_0 (see (A-11)) has perfectly rejected the interference at carrier frequency.

APPENDIX B

NOISE BANDWIDTH OF A PSEUDORANDOM PHASE-SHIFT-KEYED SIGNAL

Let $s(\cdot)$ be as in (9) with $\theta(t) \equiv 0$ and $S(t) = \pm A$, where $S(\cdot)$ changes sign every δ s in a pseudorandom manner. The noise bandwidth of such a signal, or of a filter matched to it, is defined [7, p. 201] as

$$W \triangleq \frac{\int_0^\infty |\hat{S}(f)|^2 df}{\max |\hat{S}(f)|^2} \quad (\text{B-1})$$

where $\hat{S}(\cdot)$ is the Fourier transform of $s(\cdot)$. This is the bandwidth of an ideal rectangular-band filter which has the same maximum gain as the matched filter, and whose output noise power in response to a white noise input is the same as that of the matched filter.

By Parseval's theorem, the numerator of (B-1) becomes

$$\int_0^\infty |\hat{S}(f)|^2 df = \frac{1}{2} \int_0^T s^2(t) dt = \frac{\delta}{2}. \quad (\text{B-2})$$

Since $|\hat{S}(\cdot)|^2$ is the Fourier transform of $r(\cdot)$ of (A-4), the denominator of (B-1) can be expressed as

$$\max |\hat{S}(f)|^2 = \max_f \int_{-T}^T r(\tau) \cos 2\pi f \tau d\tau \quad (\text{B-3})$$

where we have used the fact that $r(\tau)$ is even in τ and zero for $|\tau| > T$. For a phase-shift-keyed signal, $r(\cdot)$ must be amplitude-modulated form;

$$r(\tau) = R(\tau) \cos 2\pi f_0 \tau. \quad (\text{B-4})$$

We postulate a perfectly triangular mainlobe, as in (A-4);

$$R(\tau) = \delta \left(1 - \frac{|\tau|}{\delta}\right), \quad \text{for } |\tau| \leq \delta. \quad (\text{B-5})$$

The remainder of $R(\cdot)$ is heavily dependent on the particular pseudorandom sequence used but is subject to (A-11);

$$\begin{aligned} |\hat{S}(f_0)|^2 &= \int_{-T}^T r(\tau) \cos 2\pi f_0 \tau d\tau \\ &\cong \frac{1}{2} \int_{-T}^T R(\tau) d\tau = \left(\frac{A}{2} Q \delta\right)^2. \end{aligned} \quad (\text{B-6})$$

Letting L be the number of δ -s "chips" in the pseudorandom sequence ($T = L\delta$), noting that $Q = 0$ when L is even and $Q = \pm 1$ when L is odd, and using (9) in (5) with $S(t) = \pm A$ to show that $\delta = A^2 T/2 = A^2 L\delta/2$, we can proceed from (B-5) and (B-6) to find that $R(\tau)$, $\delta < |\tau| \leq T$, is constrained by

$$2 \int_\delta^T R(\tau) d\tau = \begin{cases} -\delta, & L \text{ even} \\ -\delta \left(1 - \frac{1}{L}\right), & L \text{ odd.} \end{cases} \quad (\text{B-7})$$

If we assume that $R(\tau)$ is more or less flat over $\delta < |\tau| \leq T$ (cf. [2], Figs. 17 and 18) and that $L \gg 1$, we have

$$R(\tau) \cong 1 - \frac{\delta}{2L}, \quad \text{for } \delta < |\tau| \leq T. \quad (\text{B-8})$$

The Fourier transform of the $R(\cdot)$ given by (B-5) and (B-8) is approximately

$$\hat{R}(f) \cong \delta \left[\left(\frac{\sin \pi f \delta}{\pi f \delta} \right)^2 - \frac{\sin 2\pi f L \delta}{2\pi f L \delta} \right] \quad (\text{B-9})$$

whence, using (B-4),

$$|\hat{S}(f)|^2 = \frac{1}{2} [\hat{R}(f - f_0) + \hat{R}(f + f_0)]. \quad (\text{B-10})$$

Thus $|\hat{S}(f)|^2$ is approximately a $(\sin x/x)^2$ function of width $1/\delta$, centered at f_0 , with a notch at f_0 of width $1/2L\delta$. The maximum value of $|\hat{S}(f)|^2$, which occurs just outside the notch, therefore has approximate value

$$\max |\hat{S}(f)|^2 \cong \delta/2 \quad (\text{B-11})$$

whence, from (B-1) and (B-2),

$$W \cong 1/\delta. \quad (\text{B-12})$$

APPENDIX C SNR FOR A SQUARE-LAW NONCOHERENT MATCHED FILTER

When $\text{SNR}_o \gg 1$, then $I_1(0) \gg I_2(0)$ in (13); so $y_e(T) \geq 0$ with high probability. Then we can write

$$y_e(T) \cong \frac{1}{2} [I_1(0) + I_2(0)]. \quad (\text{C-1})$$

Assuming that $N(\cdot)$ in (11) has zero mean, we have

$$E_S(y_e) \cong \frac{1}{2} I_1(0) \quad (\text{C-2})$$

$$E_{NS}(y_e) \cong 0 \quad (\text{C-3})$$

$$\text{var}_S(y_e) \cong \frac{1}{4} \bar{I}_2^2(0) \quad (\text{C-4})$$

where the overbar denotes "mean value of;" so (3) becomes

$$\text{SNR}_o(y_e) \cong \frac{I_1^2(0)}{I_2^2(0)}. \quad (\text{C-5})$$

From (12b), we can also write¹⁹

$$z = y_e^2(T) = \frac{1}{4} [I_1^2(0) + 2I_1(0)I_2(0) + I_2^2(0) + I_4^2(0)] \quad (\text{C-6})$$

¹⁹ There is some inconsistency in including the $I_4^2(0)$ term in (C-6) but not in (C-1). In defense of this, we can only say that it is tractable to do so in the former case but not in the latter; so more accuracy is attained in the results for z than in those for y_e .

from which it follows that

$$E_S(z) = \frac{1}{4} [I_1^2(0) + \overline{I_2^2(0)} + \overline{I_4^2(0)}] \quad (C-7)$$

$$E_{NS}(z) = \frac{1}{4} [\overline{I_2^2(0)} + \overline{I_4^2(0)}] \quad (C-8)$$

and

$$\text{var}_S(z) = \frac{1}{16} I_1^2(0) \overline{I_2^2(0)} \left[4 + \frac{k I_2^2(0)}{I_1^2(0)} \right] \quad (C-9)$$

where k is defined by

$$\begin{aligned} k \overline{I_2^2(0)}^2 &\triangleq 4I_1(0) [\overline{I_2^3(0)} + I_2(0) \overline{I_4^2(0)}] \\ &+ \overline{I_4^4(0) - I_2^2(0)}^2 + \overline{I_4^4(0) - I_2^2(0)}^2 \\ &+ 2[\overline{I_2^2(0) I_4^2(0)} - \overline{I_2^2(0)} \overline{I_4^2(0)}]. \end{aligned} \quad (C-10)$$

Use of (C-7)–(C-9) together with (C-5) in an SNR expression like (3) for z leads to

$$\text{SNR}_o(z) \cong \frac{\text{SNR}_o(y_e)}{4 + \frac{k}{\text{SNR}_o(y_e)}}. \quad (C-11)$$

When $\text{SNR}_o(y_e) \gg 1$, equation (C-11) becomes

$$\text{SNR}_o(z) \cong \frac{1}{4} \text{SNR}_o(y_e). \quad (C-12)$$

The value of k in (C-11) can be easily evaluated if $I_2(0)$ and $I_4(0)$ are jointly Gaussian. This will occur if the channel interference itself is Gaussian or if enough independent noise samples occur in the defining integrals for $I_2(0)$ and $I_4(0)$ so that the central limit theorem holds (e.g., when the channel interference is of the incoherent constant-amplitude type). Assuming Gaussianity of $I_2(0)$ and $I_4(0)$ to obtain, and also assuming that $\overline{I_2(0) I_4(0)} = 0$ (as is the case when the channel interference is Gaussian), then $I_2(0)$ and $I_4(0)$ are independent and (C-10) is easily shown to reduce to

$$k = 4. \quad (C-13)$$

Another case in which the value of k is of interest is when the interference is of the coherent constant-amplitude type and the signal is purely amplitude modulated ($N(\tau) \equiv J$, $\phi(\tau) \equiv \phi$, and $\theta(\tau) \equiv 0$ in (11), with J nonrandom and ϕ uniformly distributed). In this case, equation (C-10) is easily shown to reduce to

$$k = 3. \quad (C-14)$$

APPENDIX D

EQUIVALENCE OF $\hat{y}_e(\cdot)$ AND $y_e(\cdot)$ FOR AM SIGNALS

Taking the input to the device in Fig. 1 to be the sum of (9) and (10), with $\theta(t) \equiv 0$ in (9), we have for the outputs of the upper and lower multipliers

$$\begin{aligned} w_u(t) &\cong \frac{1}{2} S(t) \cos \eta + \frac{1}{2} N(t) \cos \phi(t) \cos \eta \\ &- \frac{1}{2} N(t) \sin \phi(t) \sin \eta \end{aligned} \quad (D-1)$$

$$\begin{aligned} w_l(t) &\cong -\frac{1}{2} S(t) \sin \eta - \frac{1}{2} N(t) \sin \phi(t) \cos \eta \\ &- \frac{1}{2} N(t) \cos \phi(t) \sin \eta \end{aligned} \quad (D-2)$$

where the approximations mean that we have neglected terms at frequency $2\omega_0$, which will be annihilated by the low-pass matched filters following the multipliers. After passage through matched filters with impulse response $h_{lp}(\tau) =$

$S(T - \tau)$, $0 \leq t \leq T$, $w_u(\cdot)$ and $w_l(\cdot)$ become

$$v_u(t) = \frac{1}{2} [I_1(\alpha) \cos \eta + I_2(\alpha) \cos \eta + I_4(\alpha) \sin \eta] \quad (D-3)$$

$$v_l(t) = -\frac{1}{2} [I_1(\alpha) \cos \eta + I_4(\alpha) \cos \eta + I_2(\alpha) \sin \eta] \quad (D-4)$$

where $\alpha \triangleq T - \tau$ as before and I_1 , I_2 , and I_4 are defined in connection with (11). Squaring and adding $v_u(t)$ and $v_l(t)$, we obtain

$$\hat{y}_e^2(t) = \frac{1}{4} I_1^2(\alpha) + \frac{1}{2} I_1(\alpha) I_2(\alpha) + \frac{1}{4} I_2^2(\alpha) + \frac{1}{4} I_4^2(\alpha) \quad (D-5)$$

which is seen to be identical to $y_e^2(t)$ of (12a), in which $I_3(\alpha) \equiv 0$ because $\theta(t) \equiv 0$.

APPENDIX E STATISTICS OF n_{uj} AND n_{lj}

White Gaussian Interference

Suppose that the receiver's front end has noise bandwidth W , equal to the noise bandwidth of $s(\cdot)$ and hence of the associated analog matched filter. (See Appendix B.) Then, if the channel noise is white and Gaussian, with double-sided power density $N_o/2$, the DMF input noise $n(\cdot)$ is Gaussian with variance $N_o W$ and zero mean. Hence $N(t)$ and $\phi(t)$ of (10) are, respectively, Rayleigh and uniform, and are independent [7, p. 160]. From (24) and (25),

$$\begin{aligned} E[n_{uj}^2|\eta] &= \frac{1}{4} E[N^2(j\delta)] E[\cos^2(\phi(j\delta) + \eta)|\eta] \\ &= \frac{1}{8} E[N^2(j\delta)] = \frac{N_o W}{4} \end{aligned} \quad (E-1)$$

and similarly

$$E[n_{lj}^2|\eta] = \frac{N_o W}{4} \quad (E-2)$$

where we have used the fact that the mean-square envelope of a Gaussian process is twice the variance of the process itself [7, p. 160]. Clearly, n_{uj} and n_{lj} have zero mean.

Since the sets of random variables n_{u1}, \dots, n_{uL} and n_{l1}, \dots, n_{lL} result from linear operations on a Gaussian process, they are jointly Gaussian. We have from (24) and (25)

$$E[n_{uj}n_{lj}|\eta] = -\frac{1}{2} E[N^2(j\delta)] E[\sin 2(\phi(j\delta) + \eta)|\eta] = 0 \quad (E-3)$$

so n_{uj} and n_{lj} are independent.

From Appendix B, $W = 1/\delta$; and since $1/W$ is approximately the interval over which a process with noise bandwidth W decorrelates, we have that n_{uj} and n_{uk} are approximately uncorrelated, hence independent for $j \neq k$, especially for $|k - j| > 1$. A similar statement holds, for n_{lj} and n_{lk} . From these results and (E-3), it follows that $n_{u1}, \dots, n_{uL}, n_{l1}, \dots, n_{lL}$ are approximately independent Gaussian random variables.

Incoherent Constant-Amplitude Interference

From (51) and (52), the assumed independence of the $\phi(j\delta)$ dictates the independence of n_{uj} and n_{uk} , of n_{lj} and n_{lk} , and of n_{uj} and n_{lk} ($j \neq k$). Clearly, n_{uj} and n_{lj} are dependent, although uncorrelated;

$$E[n_{uj}n_{lj}|\eta] = -\frac{J^2}{2} E[\sin 2(\phi(j\delta) + \eta)|\eta] = 0. \quad (E-4)$$

Thus among the set of $2L$ variables $n_{u1}, \dots, n_{uL}, n_{l1}, \dots, n_{lL}$, only L of the $L(2L - 1)$ pairs have even a slight dependence. Any dependence between the two sums of (27) and (28) is therefore slight.

ACKNOWLEDGMENT

The author gratefully acknowledges the work of J. J. C. Chiang and R. Y. Ibaraki in writing the program used for the simulation results presented in Section VII. Their work [13] also includes simulations of DMF's with multibit digitization, to be presented elsewhere.

Thanks are also due Prof. N. T. Gaarder, T. Lim, and two anonymous reviewers for their clarifying comments on certain aspects of the original manuscript.

REFERENCES

- [1] Special Issue on Microwave Signal Processing, *IEEE Trans. Sonics Ultrason.*, vol. SU-20, Apr. 1973.
- [2] G. L. Turin, "An introduction to matched filters," *IRE Trans. Inform. Theory*, vol. IT-6, pp. 311-329, June 1960.
- [3] G. L. Turin, "Minimax strategies for matched-filter detection," *IEEE Trans. Commun.*, vol. COM-23, pp. 1370-1371, Nov. 1975.
- [4] C. R. Cahn, "Performance of digital matched filter correlator with unknown interference," *IEEE Trans. Commun. Technol.*, vol. COM-19, pp. 1163-1172, Dec. 1971, part II.
- [5] D. J. Gooding, "A Digital Matched Filter for Signals of Large Time-Bandwidth Product," Sylvania Communication Systems Laboratory, Waltham, MA, Tech. Rep. 16, Feb. 1969.
- [6] K. Y. Chang and A. D. Moore, "Modified digital correlator and its estimation errors," *IEEE Trans. Inform. Theory*, vol. IT-16, pp. 699-706, Nov. 1970.
- [7] W. B. Davenport, Jr., and W. L. Root, *An Introduction to the Theory of Random Signals and Noise*. New York: McGraw-Hill, 1958.
- [8] G. L. Turin, "Communication through noisy, random-multipath channels," *IRE Conv. Rec.*, vol. 4, part IV, pp. 154-166, 1956.
- [9] G. L. Turin, *Notes on Digital Communication*. New York: Van Nostrand Reinhold, 1969.
- [10] E. Parzen, *Modern Probability Theory and Its Applications*. New York: Wiley, 1960.
- [11] D. J. Gooding, "Increasing the Utility of the Digital Matched Filter," Stein Assoc., Waltham, MA, Tech. Note 71-4, June 1971.
- [12] D. J. Gooding, "Increasing the utility of the digital matched filter," in *NELC Spread Spectrum Symp. Proc.*, 1973.
- [13] J. J. C. Chiang and R. Y. Ibaraki, "Digital Matched Filter Simulation," M.S. project report, Dept. Elec. Eng. and Computer Sci., Univ. of California, Berkeley, CA, Jan. 1975.
- [14] S. W. Golomb, *Shift Register Sequences*. San Francisco: Holden-Day, 1967.